Geochemistry Geophysics Geosystems G3

Article
Volume 11, Number 5
25 May 2010
Q05006, doi:10.1029/2010GC003064
ISSN: 1525-2027

Published by AGU and the Geochemical Society

Origin of volcanic seamounts at the continental margin of California related to changes in plate margins

A. S. Davis, D. A. Clague, and J. B. Paduan
MBARI, 7700 Sandholdt Road, Moss Landing, California 95039, USA (clague@mbari.org)

B. L. Cousens
Department of Earth Sciences, Carleton University, 1125 Colonel By Drive, Ottawa, Ontario K1S 5B6, Canada

J. Huard
Department of Oceanic and Atmospheric Science, Oregon State University, Corvallis, Oregon 97331, USA

[1] Volcanic samples collected with the Monterey Bay Aquarium Research Institute's ROV *Tiburon* from eight seamounts at the continental margin offshore central to southern California comprise a diverse suite of mainly alkalic basalt to trachyte but also include rare tholeiitic basalt and basanite. All samples experienced complex crystal fractionation probably near the crust/mantle boundary, based on the presence in some of mantle xenoliths. Incompatible trace elements, poorly correlated with isotopic compositions, suggest variable degrees of partial melting of compositionally heterogeneous mantle sources, ranging from MORB-like to relatively enriched OIB. High-precision $^{40}Ar/^{39}Ar$ ages indicate episodes of volcanic activity mainly from 16 to 7 Ma but document one eruption as recent as 2.8 Ma at San Juan Seamount. Synchronous episodes of volcanism occurred at geographically widely separated locations offshore and within the continental borderland. Collectively, the samples from these seamounts have age ranges and chemical compositions similar to those from Davidson Seamount, identified as being located atop an abandoned spreading center. These seamounts appear to have a common origin ultimately related to abandonment and partial subduction of spreading center segments when the plate boundary changed from subduction-dominated to a transform margin. They differ in composition, age, and origin from other more widespread near-ridge seamounts, which commonly have circular plans with nested calderas, and from age progressive volcanoes in linear arrays, such as the Fieberling-Guadalupe chain, that occur in the same region. Each volcanic episode represents decompression melting of discrete enriched material in the suboceanic mantle with melts rising along zones of weakness in the oceanic crust fabric. The process may be aided by transtensional tectonics related to continued faulting along the continental margin.

Components: 29,000 words, 13 figures, 5 tables.

Keywords: seamounts; chemistry; Ar-Ar age dates.

Index Terms: 8427 Volcanology: Subaqueous volcanism; 8416 Volcanology: Mid-oceanic ridge processes (1032, 3614); 8415 Volcanology: Intra-plate processes (1033, 3615).

Received 28 January 2010; **Accepted** 4 February 2010; **Published** 25 May 2010.

Davis, A. S., D. A. Clague, J. B. Paduan, B. L. Cousens, and J. Huard (2010), Origin of volcanic seamounts at the continental margin of California related to changes in plate margins, *Geochem. Geophys. Geosyst.*, *11*, Q05006, doi:10.1029/2010GC003064.

1. Introduction

[2] Many volcanic seamounts offshore central to southern California, as elsewhere, do not fit the classical hot spot or plume model for the origin of ocean island volcanoes. The ones offshore California are complex, elongated structures with a distinctive NE-SW alignment (Figure 1) built by many small volume eruptions that are roughly synchronous at widely scattered locations [*Davis et al.*, 1995, 2002]. Our previous studies, suggesting that these volcanoes represent a different kind of intraplate volcanism, were based on a limited number of poorly located dredge samples [*Davis et al.*, 1995] and a few dive samples [*Davis et al.*, 2002]. To date, the Monterey Bay Aquarium Research Institute (MBARI) has conducted 54 dives with ROV *Tiburon* to nine seamounts to collect well-located samples, combined with bottom observations. From the hundreds of samples collected between 37.5°N and 32.3°N, four hundred and twenty-one volcanic rock and breccia samples were analyzed for whole rock and/or glass compositions. The chemistry and ages of the samples allow us to evaluate whether seamounts clearly not arranged in linear chains also evolve through a series of growth stages as seen in volcanoes from linear age progressive chains such as Hawaii [e.g., *Clague and Dalrymple*, 1987] or Jasper Seamount in the Fieberling-Guadalupe chain [*Konter et al.*, 2009].

[3] Only Davidson and Guide Seamounts have been identified as straddling abandoned spreading centers, based on magnetic anomalies [*Lonsdale*, 1991; *Castillo et al.*, 2010]. Whole-rock major and trace element, and Sr, Nd, Pb isotopic geochemistry of samples from Davidson are reported by *Castillo et al.* [2010] and radiometric ages and glass chemistry of dive samples from Davidson are described by *Clague et al.* [2009b]. Here we present new $^{40}Ar/^{39}Ar$ ages, rock and glass chemistry, and Sr, Nd, and Pb isotope compositions of subsets of the 324 samples from the other eight sites. We compare the chemistry with that of samples from Davidson and other seamounts built atop abandoned spreading centers and we interpret the geologic history within the context of the complex tectonics of coastal California.

2. Geologic Setting

[4] All of the seamounts are complex, elongated structures with a distinctive northeast to southwest orientation common to many other volcanic edifices near the continental margins of Southern and Baja California [*Atwater and Severinghaus*, 1989]. Seven of the nine volcanic seamounts (Guide, Gumdrop, Pioneer, Davidson, San Juan, San Marcos, Little Joe) are located on the Pacific plate (Figure 1); Rodriguez is located on the continental slope; and Northeast Bank is located within the Continental Borderland (Figure 1). San Juan, about 30 km wide and 70 km long, is the largest of these volcanoes. San Marcos is similar in size to Davidson (~14 km by 42 km) but the others are smaller (~12 to 16 km long). Although variable in size, all of the seamounts have a similar morphology, consisting of 4 to 6 parallel ridges separated by sediment-filled troughs. Small irregular cones are aligned along the ridges, but none of these cones have craters at their summits. Rodriguez and Northeast Bank have flat tops surrounded by beach deposits indicating they were islands [*Paduan et al.*, 2009]. These two reach the shallowest depths at 675 and 516 m. The others have summits typically near to, or deeper than 1000 m (Table A1), although high vesicle abundance and low sulfur content of glasses from volcaniclastic breccias suggest many eruptions occurred in water depths considerably shallower than their present depths [*Davis and Clague*, 2003].

[5] These seamounts differ in morphology from near-ridge seamounts [e.g., *Clague et al.*, 2000] that have generally circular plan and nested large calderas. Examples in this region, such as Hoss and Ben [*Davis et al.*, 1995] and Bonanza, Hop-Sing, Echo, and Linzer seamounts [*Konter et al.*, 2009], also are characterized by strongly depleted mid-ocean ridge basalt (MORB) compositions. They also differ in morphology and origin from volcanoes such as Jasper arrayed in linear chains like the Fieberling-Guadalupe chain [*Gee et al.*, 1991; *Konter et al.*, 2009] that are also generally circular in shape with flat or domed summits.

[6] Magnetic anomalies of Chron 6, ~20 Ma in age [*Atwater and Severinghaus*, 1989; *Lonsdale*, 1991] occurring symmetrically on both sides of Davidson and Guide, indicate they are built on top of fossil spreading centers [*Davis et al.*, 2002, Figure 2; *Castillo et al.*, 2010, Figure 1]. Magnetic anomalies near Gumdrop and Pioneer are not mapped as symmetrical but correspond to Chron 6B to 6C indicating ocean crust of about 22 to 24 Ma. Magnetic anomalies near the other seamounts become younger southward: Chron 6–6A near San Marcos, Chron 6–5E near San Juan, and Chron 5D near Little Joe, which correspond to ages between about 22 and 18 Ma. Magnetic anomalies

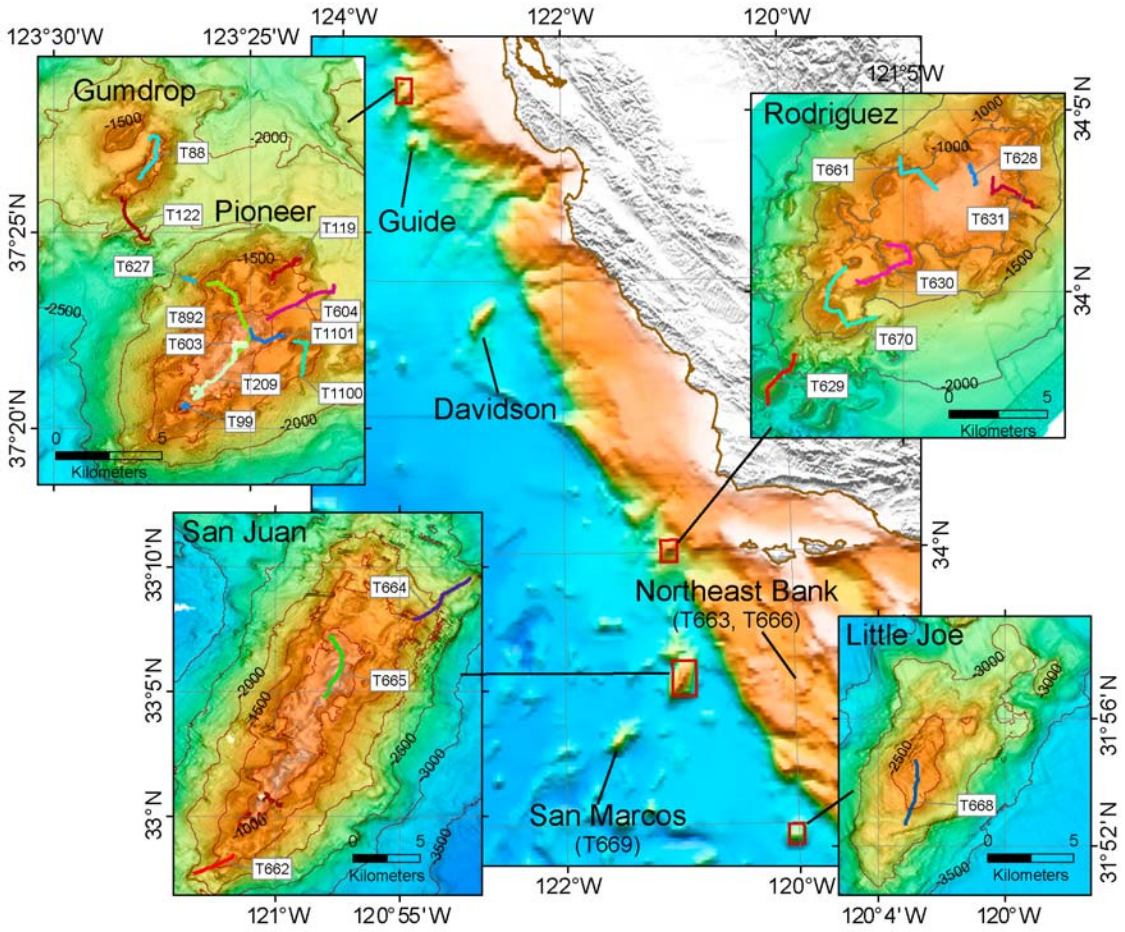

Figure 1. Bathymetric map shows location of the seamounts relative to the continental margin. Insets show five of the seamounts with ROV dive tracks. EM 300 multibeam sonar bathymetric images of Guide, Pioneer, Gumdrop, and Rodriguez are presented by *Davis et al.* [2002] and, along with bathymetry of Davidson, are from *MBARI Mapping Team* [2001]. Contour interval is 500 m. Note that Northeast Bank and San Marcos Seamount have only partial multibeam coverage.

outboard from Rodriguez are of Chron 5E or 19 Ma in age [*Atwater and Severinghaus*, 1989].

3. Sampling and Analytical Methods

[7] All dive samples were collected on cruises of MBARI's R/V *Western Flyer* with remotely operated vehicle (ROV) *Tiburon.* Samples labeled T88 to T124 were collected from Guide, Gumdrop, and from Pioneer in 1998 and 2000 [*Davis et al.*, 2002]. Additional samples were collected on Pioneer during dives T603 and T604 in 2003, on dive T892 in 2005, and dives T1100 and T1101 in 2007. Dive samples from the seamounts offshore southern California were collected in 2003, 2004, 2006, and 2007. Locations and water depths for collected samples are given in Table A1. Four of the dive samples are gravel collected either with push cores (PCxx) or sediment scoop bags (SBxx); all others were picked up with the manipulator arm. Because of the presence of erratics on all of the seamounts [*Paduan et al.*, 2007], we typically took multiple samples at a given site and tried to break off outcrop, whenever possible. Additional samples from Northeast Bank [*Hawkins et al.*, 1971] were obtained from Scripps Oceanographic Institute's dredge collection of the 1969 cruise of the R/V *Agassiz* (AGD3-x).

[8] The rocks were cut for thin sections and the least altered material was selected for major and select trace element analyses by XRF and rare earth and additional trace elements by ICP-MS in the GeoAnalytical Laboratory of Washington State University. Information on methods, precision, and accuracy are given by *Johnson et al.* [1999] and *Knaack et al.* [1994]. Polished thin sections of

168 samples with fresh glass, either from glass rinds or more commonly volcaniclastic breccia or turbidite sand, were analyzed with a JEOL 8900 Superprobe at the U.S. Geological Survey in Menlo Park, CA. Analyses were performed with 15 kv accelerating voltage, 20 nAmps specimen current, using a 10 μm beam size and natural and synthetic glass and mineral standards [e.g., *Davis et al.*, 1994]. Each analysis is typically the average of five or more points.

[9] Based on thin section examination, 47 samples were selected for radiometric dating. For 38 samples with abundant, unaltered plagioclase the age measurements were performed on acid-treated mineral separates, using techniques described by *Koppers et al.* [2000]. For sparsely phyric, or aphyric samples, age determinations were made on either crystalline groundmass separates (2 samples) or on minicores of the least altered part of whole rocks (5 samples), following methods described by *Duncan and Keller* [2004]. Plagioclase and crystalline groundmass separates were analyzed using a CO_2 laser probe [*Koppers et al.*, 2003] and whole rock disks by incremental heating with a double-vacuum resistance furnace [*Duncan and Keller*, 2004]. All samples were irradiated in Oregon State University's TRIGA reactor for 6 h, using the flux monitor standard FCT-3 biotite. Details of the irradiation, calibration, and age calculations are described by *Koppers et al.* [2003].

[10] Radiogenic isotope compositions of Sr, Nd, and Pb of 33 selected samples were determined by thermal ionization mass spectrometry at Carleton University, Ottawa, utilizing techniques described by *Cousens* [1996]. Prior to dissolution, splits for Pb and Nd were acid-washed in warm 1.5N HCl for 12 h, then rinsed three times with ultrapure H_2O. Splits for Sr were acid-washed in hot 6N HCl for 4 days, then rinsed three times with H_2O, followed by dissolution in HF/HNO_3. All Pb mass spectrometer runs are corrected for fractionation using NIST SRM981. The average ratios measured for SRM981 are $^{206}Pb/^{204}Pb$ = 16.890 ± 0.010, $^{207}Pb/^{204}Pb$ = 15.429 ± 0.013, and $^{208}Pb/^{204}Pb$ = 36.502 ± 0.042 (2 sigma). The fractionation correction, based on the values of *Todt et al.* [1984], is ±0.13%/amu. Sr isotope ratios are normalized to $^{86}Sr/^{88}Sr$ = 0.11940 to correct for fractionation. Two Sr standards are run at Carleton, NIST SRM987 ($^{87}Sr/^{86}Sr$ = 0.710251 ± 18) and the Eimer and Amend (E&A) $SrCO_3$ ($^{87}Sr/^{86}Sr$ = 0.708032 ± 24). Nd isotope ratios are normalized to $^{146}Nd/^{144}Nd$ = 0.72190.54 runs of the La Jolla standard average $^{143}Nd/^{144}Nd$ = 0.511876 ± 18.

4. Results

4.1. Sample Descriptions

[11] The samples collected from the seamounts are a diverse suite of basaltic lavas and volcaniclastic breccias and sandstones. Location, water depths, and rock types for all samples are given in Table A1. Analyses of 13 samples from Guide, 10 from Gumdrop, and 7 samples from Pioneer are published (references in Table A1). The analyses of these are not repeated in Tables 1, 2, A2, and A3, but are included in Figures 2–13.

[12] Rocks collected from all of the seamounts are similar, with hawaiite and alkalic basalt being the most common rock types (Figure 2, classification of *Cox et al.* [1979]). Mugearites occur at most sites but more evolved benmoreite and trachyte were only recovered from Rodriguez, which, next to Davidson, is the most intensively sampled of these sites. Tholeiitic and transitional basalt, in addition to alkalic basalt and hawaiite, were collected on Little Joe and basanite was collected in addition to alkalic basalt and hawaiite on San Juan. The alkalic basalt and hawaiite from all sites are typically highly vesicular, with small round or elongated vesicles that often show flow alignment. Numerous samples from Rodriguez and Northeast Bank are extremely vesicular whereas some basalt samples from San Marcos, Little Joe, and from the deeper dive on San Juan are nearly vesicle free. Most of the basalt and hawaiite are sparsely to moderately porphyritic with plagioclase as the dominant phenocryst phase, accompanied by variable amounts of olivine and clinopyroxene. The olivine is mostly replaced by iddingsite and clay, although fresh cores remain in many samples. Unlike the other seamount samples, the olivine in the samples from Little Joe consists of unaltered, euhedral, microphenocrysts, accompanied by various amounts of plagioclase microlites.

[13] Plagioclase, and more rarely clinopyroxene, in the alkalic samples reach cm size and many are complexly zoned. Brown amphibole is present in mugearite from Pioneer and San Juan and pale green aegerine-augite is present in the trachyte from Rodriguez. Numerous samples, especially from Rodriguez but also from Pioneer and San Juan, contain xenoliths of anorthosite, gabbro, and

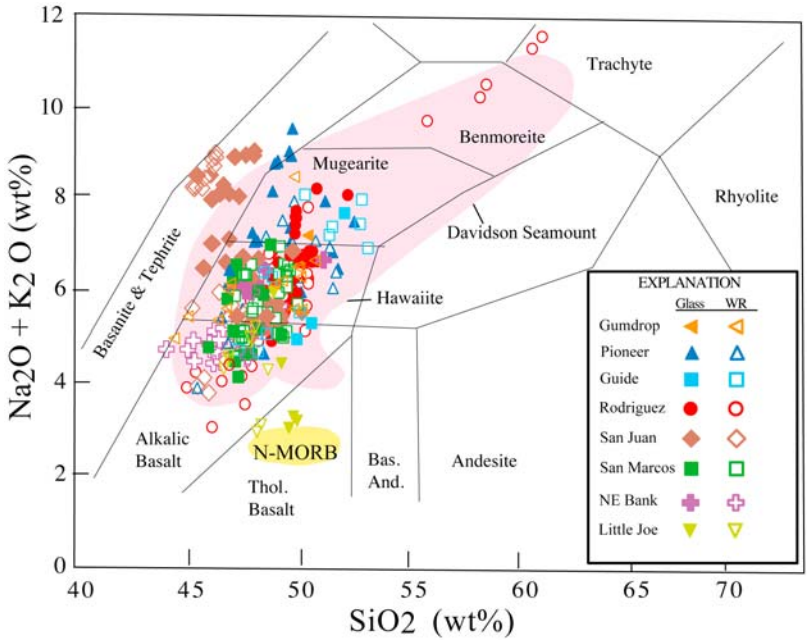

Figure 2. Alkalis versus silica plot shows the range of whole-rock (open symbols) and glass compositions (filled symbols) for the seamounts. Fields for Davidson Seamount [*Castillo et al.*, 2010; *Clague et al.*, 2009b; *Davis et al.*, 2002] and N-MORB from Gorda Ridge [*Davis and Clague*, 1987, 1990; *Davis et al.*, 2008] are shown for comparison. Data are normalized to 100%. Rock classification of *Cox et al.* [1979].

dunite. Definite mantle xenoliths of lherzolite are only found in rare Rodriguez basalt. These xenoliths are similar to, but not nearly as abundant, as those from Davidson [*Davis et al.*, 2007]. No kaersutite megacrysts or biotite, distinctive among Davidson xenoliths, were found among these xenoliths. Care was taken to avoid visible xenoliths in the analyzed splits, but it is uncertain if some of the complexly zoned phenocrysts are disaggregated xenoliths.

[14] Despite extensive secondary alteration of much of the interstitial glass, fresh glass rims many samples and occurs in volcaniclastic breccias and sandstones. Fresh glass cores in volcanic breccias are typically rimmed by palagonite, which in many samples completely replaces the glass. The volcaniclastic samples have a large variety of textures, including highly vesicular lapilli tuffs with rounded or angular vesicles, scoria clasts, and graded and bedded turbidite and sandstones [*Davis and Clague*, 2003]. The volcaniclastic sample (T668R18) from Little Joe Seamount is hyaloclastite with dense angular glass fragments, that resembles those described from near-ridge seamounts [e.g., *Batiza and Vanko*, 1984; *Davis and Clague*, 2000; *Smith and Batiza*, 1989]. The range of compositions of the whole-rock samples, including tholeiitic and alkalic basalt, hawaiite, mugearite, and basanite, are also present as glass rinds and fragments, but groundmass glass of the benmoreite and trachyte are too crystal-rich to analyze. Problems related to secondary alteration and potential inclusion of xenocrysts will be discussed in section 4.3.

4.2. Ages of Rocks

[15] New high-precision $^{40}Ar/^{39}Ar$ ages for 47 samples are given in Table 1 (full Ar-Ar analytical details for each sample are available at http://www.mbari.org/volcanism/SouthernCaliforniaSeamountsMS/default.htm). Despite variable secondary alteration in many samples, most of the analyses yield well-defined plateau ages that, at the 95% level of confidence, are concordant with the inverse isochron ages and most have atmospheric $^{40}Ar/^{39}Ar$ intercepts. Many of the total fusion ages are in agreement with the plateau and isochron ages, while others are significantly older. The only strongly discordant age is for sample T603R7 from Pioneer (Table 1). We use the plateau ages to best represent the crystallization ages of the samples.

[16] Ages of four alkalic basalts from Gumdrop range from 15.0 ± 0.32 to 16.4 ± 0.32 Ma, spanning a minimum of 1.4 ± 0.6 million years of volcanism. The older age is similar to that previously published for four samples from Guide

Table 1. The $^{40}Ar/^{39}Ar$ Radiometric Age Determinations[a]

Sample	Material	Total Fusion Age ± 2σ (Ma)	Plateau				Isochron	
			Age ± 2σ	Steps[b]	^{39}Ar[b]	MSWD	Age ± 2σ	$^{40}Ar/^{36}Ar$ ± 2σ
Gumdrop Seamount								
T122R2	plagioclase	22.35 ± 0.39	14.97 ± 0.32	4/8	77.8	0.14	14.99 ± 0.32	291.5 ± 15.1
T122R5	plagioclase	24.14 ± 0.35	15.20 ± 0.29	4/8	80.5	0.07	15.12 ± 0.61	316.5 ± 139.9
T122R9	plagioclase	19.45 ± 0.32	15.01 ± 0.29	5/8	89.0	0.64	14.99 ± 0.30	299.3 ± 15.3
T122R19	plagioclase	16.49 ± 0.37	16.43 ± 0.32	8/8	100.0	0.82	16.33 ± 0.37	298.2 ± 6.7
Pioneer Seamount								
T99R1	groundmass	11.02 ± 0.22	11.51 ± 0.16	4/8	84.0	0.49	11.51 ± 0.17	296.4 ± 6.3
T119R11	plagioclase	11.19 ± 0.22	11.19 ± 0.21	8/8	100.0	0.12	11.18 ± 0.23	298.2 ± 17.7
T119R15	plagioclase	11.40 ± 0.19	11.20 ± 0.18	6/7	94.6	0.08	11.19 ± 0.20	298.3 ± 24.3
T603R6	plagioclase	64.55 ± 16.41	36.36 ± 23.20	4/9	70.3	1.34	55.92 ± 44.46	292.8 ± 6.7
T604R8	plagioclase	18.63 ± 0.18	13.01 ± 0.16	3/7	67.3	0.72	12.98 ± 0.17	300.7 ± 9.2
T627R2	plagioclase	11.18 ± 0.13	10.94 ± 0.13	5/8	79.4	0.83	10.94 ± 0.14	297.8 ± 12.3
T627R5	plagioclase	11.76 ± 0.21	11.30 ± 0.20	5/8	78.2	0.86	11.29 ± 0.21	297.8 ± 10.0
T1100R2	plagioclase	14.86 ± 0.38	11.95 ± 0.31	3/8	55.8	1.03	11.90 ± 0.48	301.0 ± 27.1
T1100R2	groundmass	11.98 ± 0.16	11.96 ± 0.11	4/11	66.1	1.16	11.87 ± 0.18	300.8 ± 8.9
T1100R7	plagioclase	13.21 ± 0.41	11.66 ± 0.35	4/8	67.5	0.43	11.56 ± 0.48	301.5 ± 20.5
T1100R7	groundmass	12.40 ± 0.22	12.19 ± 0.08	5/12	77.2	0.69	12.18 ± 0.09	296.7 ± 4.6
T1101R6	plagioclase	11.09 ± 0.11	10.96 ± 0.09	9/11	93.6	0.5	10.94 ± 0.16	298.1 ± 12.1
Rodriguez Seamount								
T628R1	plagioclase	15.71 ± 0.21	9.85 ± 0.17	5/8	70.5	1.20	9.80 ± 0.20	305.5 ± 22.0
T628R11	plagioclase	15.48 ± 0.22	9.90 ± 0.17	4/8	62.5	0.20	9.89 ± 0.20	297.7 ± 29.4
T629R24	plagioclase	11.73 ± 0.18	11.55 ± 0.15	8/9	97.3	0.84	11.42 ± 0.25	309.4 ± 19.5
T630R14	plagioclase	10.30 ± 0.17	10.35 ± 0.25	6/7	96.1	2.42	10.08 ± 0.27	321.1 ± 19.0
T630R28	plagioclase	11.02 ± 0.18	10.22 ± 0.17	5/7	94.5	0.45	10.17 ± 0.19	306.4 ± 19.1
T630R31	plagioclase	11.55 ± 0.21	11.53 ± 0.19	9/9	100.0	0.41	11.48 ± 0.22	299.7 ± 10.3
T631R11	plagioclase	9.65 ± 0.22	9.71 ± 0.34	5/8	78.9	2.04	9.44 ± 0.36	331.7 ± 31.8
T631R17[c]	plagioclase	18.07 ± 0.41	17.87 ± 0.36	6/7	93.1	1.02	18.15 ± 0.54	289.1 ± 9.3
T631R30	plagioclase	10.06 ± 0.19	9.99 ± 0.18	4/8	93.2	0.60	10.06 ± 0.21	241.2 ± 23.6
T631R41	plagioclase	9.86 ± 0.27	9.72 ± 0.21	7/8	99.6	0.34	9.71 ± 0.22	296.0 ± 4.0
T661R13	plagioclase	10.42 ± 0.17	10.47 ± 0.15	9/9	100.0	0.83	10.36 ± 0.17	303.9 ± 8.2
T661R19	plagioclase	10.71 ± 0.24	10.74 ± 0.22	8/8	100.0	0.50	10.70 ± 0.27	297.5 ± 8.1
T670R1[c]	plagioclase	10.25 ± 0.22	10.27 ± 0.22	8/8	100.0	1.13	10.14 ± 0.23	309.9 ± 13.1
T670R18	plagioclase	11.11 ± 0.22	10.98 ± 0.22	7/8	95.6	0.45	10.94 ± 0.28	298.2 ± 13.0
T670R27	plagioclase	11.24 ± 0.23	11.25 ± 0.23	8/8	100.0	0.40	11.24 ± 0.26	297.4 ± 14.3
T670R32	whole rock	11.70 ± 0.09	11.71 ± 0.10	3/10	65.1	3.35	11.61 ± 0.19	370.5 ± 118.9
T670R39	whole rock	11.19 ± 0.08	11.14 ± 0.08	8/10	94.8	0.42	11.14 ± 0.08	298.7 ± 7.4
San Juan Seamount								
T662R11	plagioclase	10.59 ± 0.17	10.22 ± 0.21	5/7	88.6	1.93	10.25 ± 0.26	291.1 ± 13.9
T664R7	whole rock	2.66 ± 0.05	2.69 ± 0.05	5/10	79.6	1.89	2.73 ± 0.03	290.6 ± 5.3
T664R27[c]	plagioclase	18.70 ± 0.45	18.72 ± 0.42	8/8	100.0	0.62	18.43 ± 0.61	300.9 ± 7.8
T665R33	plagioclase	10.65 ± 0.23	10.65 ± 0.22	8/8	100.0	0.40	10.61 ± 0.24	303.2 ± 14.2
San Marcos Seamount								
T669R1	plagioclase	16.81 ± 0.44	6.71 ± 0.33	4/7	86.4	2.19	6.60 ± 0.25	299.9 ± 3.7
T669R16	plagioclase	10.23 ± 0.17	9.70 ± 0.18	5/8	81.2	1.71	9.58 ± 0.25	311.4 ± 13.5
T669R20	plagioclase	10.27 ± 0.49	10.12 ± 0.30	5/8	81.4	1.52	10.19 ± 0.32	293.6 ± 3.7
T669R27	plagioclase	11.46 ± 0.21	9.73 ± 0.21	5/8	71.7	1.06	9.71 ± 0.21	299.0 ± 6.8
Northeast Bank								
T663R13	plagioclase	13.19 ± 0.34	8.76 ± 0.33	4/7	47.1	0.64	8.59 ± 0.43	301.2 ± 9.4
T663R15	plagioclase	14.25 ± 0.29	7.15 ± 0.27	4/8	78.0	0.05	7.14 ± 0.42	295.6 ± 16.6
T666R34	groundmass	7.63 ± 0.18	7.03 ± 0.11	6/8	83.4	0.97	6.97 ± 0.13	300.3 ± 5.3
T666R38	plagioclase	8.04 ± 0.31	7.24 ± 0.30	5/7	64.2	0.06	7.25 ± 0.37	294.5 ± 13.4
Little Joe Seamount								
T668R7	whole rock	14.08 ± 0.16	none					
T668R17	whole rock	10.25 ± 0.05	11.06 ± 0.07	5/11	53.5	2.39	11.03 ± 0.14	306.5 ± 41.8

[a] Samples irradiated at OSU TRIGA reactor for 6 h at 1MW power. Neutron flux measured using FCT-3 biotite monitor [*Renne et al.*, 1998]. Data reduced by ArArCALC software [*Koppers*, 2002].
[b] Plateau age data includes number of steps in the plateau (steps in plateau/total steps) and % ^{39}Ar in plateau.
[c] Erratic calc-alkaline lava. See Data Set S2 for chemistry.

of 16.58 ± 0.5 Ma [*Davis et al.*, 2002]. Besides the highly discordant age for T603R7, nine other samples from Pioneer have concordant plateau and isochron ages, ranging from 10.94 ± 0.13 Ma to 13.01 ± 0.16 Ma (Table 1). Total fusion ages are in agreement for all except two samples, which have fusion ages that are significantly older (to 18.6 Ma). These ages are in good agreement with the previously dated alkalic basalt and hawaiite from Pioneer at 11.01 ± 0.14 Ma [*Davis et al.*, 2002]. Volcanism at Pioneer lasted for at least 2.1 ± 0.3 million years.

[17] Seventeen samples, including alkalic basalt, hawaiite, benmoreite, and trachyte, were dated from Rodriguez. The alkalic basalt and hawaiite were analyzed as plagioclase separates; the two analyzed whole rock cores are benmoreite and trachyte. All plateau and isochron ages are concordant but several of the total fusion ages are significantly older. Samples T631R17 (17.87 ± 0.36 Ma) and T670R1 (10.25 ± 0.22 Ma) have calc-alkaline compositions and are interpreted to be erratics despite the similar age of T670R1 to the in situ samples. The total age range is from 9.71 ± 0.21 Ma to 11.71 ± 0.10 Ma. The trachyte is near the older end of the age spectrum (i.e., 11.7 Ma). The large number of reliable ages suggests that volcanic activity spanned a period of at least 2 ± 0.3 million years. Ages for plagioclase separates from dredge samples of 9.44 ± 0.14 Ma [*Davis et al.*, 2002] and 12.0 ± 0.4 Ma [*Davis et al.*, 1995] roughly bracket the new ages and extend duration of volcanism to 2.6 ± 0.5 million years.

[18] From the four samples dated from San Juan, the oldest one (T664R27) with an age of 18.70 ± 0.42 Ma is also a calc-alkaline erratic. The plagioclase separates from alkalic basalt and hawaiite gave ages of 10.22 ± 0.21 and 10.65 ± 0.22, respectively. The plateau, isochron, and total fusion ages are all concordant. The basanite gave a young age of 2.69 ± 0.05 Ma. Because the basanite samples have virtually no secondary alteration, high K_2O contents, and all three measures of ages are concordant and with atmospheric intercept we consider this age to be reliable. Volcanism therefore persisted on San Juan for 8 ± 0.3 million years.

[19] The four separates of plagioclase from alkalic basalt and hawaiite from San Marcos gave ages ranging from 6.71 ± 0.33 Ma to 10.12 ± 0.30 Ma. Plateau and isochron ages are concordant but two of the total fusion ages are significantly older (Table 1). Two relatively imprecise ages for dredge samples from San Marcos of 11 ± 2 Ma and 16.0 ± 1 Ma [*Davis et al.*, 1995] may suggest an older episode of volcanism at this site. The older sample is a hawaiite comparable to the other seamount lavas and cannot be a subaerially erupted erratic because it has a glass rim. Collectively, these data indicate that volcanism at San Marcos persisted for at least 3.4 ± 0.6 million years, but probably as long as 9.3 ± 1.3 million years.

[20] For Northeast Bank, three plagioclase samples and one groundmass separate gave ages ranging from 7.03 ± 0.11 Ma to 8.76 ± 0.33 Ma. Plateau and isochron ages are concordant but two of the total fusion ages are older. Previously published ages of dredged samples of 9.3 ± 0.1 and 11.5 ± 0.1 Ma [*Bohrson and Davis*, 1994] also suggest older volcanism at this site. Volcanism persisted at this site for at least 1.7 ± 0.4 and perhaps as long as 4.5 ± 0.2 million years.

[21] Samples from Little Joe were more difficult to date because of low K_2O contents and more extensive alteration. They include the lowest-K_2O (0.47%) sample, which did not yield a plateau age but gave a total fusion age of 14.08 ± 0.16 Ma. The other dated sample, a mildly alkalic basalt, gave a plateau age of 11.06 ± 0.07 Ma, which is concordant with the inverse isochron age and only slightly older than the total fusion age. From the age data it is not instructive to infer how long volcanic activity persisted at this site.

[22] A pattern of prolonged volcanic activity, similar to that determined here, is documented for Davidson [*Clague et al.*, 2009b], with volcanism ranging from 14.8 to 9.8 Ma, therefore persisting for at least 5.0 ± 0.3 million years.

4.3. Problems Due to Secondary Processes

[23] Unraveling the complex petrologic origin of these volcanic rocks is complicated by four factors unrelated to melt diversity. One, common with older submarine lavas, is that of secondary alteration due to oxidation and clay mineral formation in the groundmass or as vesicle fillings. Mostly, this results in greater scatter in major elements, especially in the alkalis. Care was taken to avoid altered areas for whole rock analyses but we primarily use glass analyses for considering major element trends.

[24] The second problem is secondary alteration that increases P_2O_5. This appears to be limited to samples erupted subaerially when some of the seamounts were islands [*Paduan et al.*, 2009] that may have been capped by guano deposits, analo-

gous to some modern sites (e.g., Rocas Alijos [*Davis et al.*, 1996]). Not detectable in thin sections, X-ray imaging showed the P_2O_5 to be diffused in the tachylitic groundmass of some samples [*Paduan et al.*, 2009]. Samples with extreme phosphate alteration (~3%–8.4% P_2O_5 (Data Set S1)) are omitted from Figures 2, 4, 5, 6, 9, 10, 12, and 13.[1]

[25] The third problem is the presence of xenocrysts. Samples cut for analyses were carefully selected to avoid xenoliths but, as the xenoliths from Davidson have shown, they can be disaggregated and difficult to distinguish from large complexly zoned phenocrysts [*Davis et al.*, 2007]. Since most of the phenocrysts are plagioclase, they could also affect the age determination, although this seems unlikely because the ages of any xenocrysts would also be reset when the host magma cooled. Plagioclase xenocrysts are typically more evolved than phenocrysts in their host lava and some contain magmatic apatite [*Davis et al.*, 2007] that may also affect P_2O_5 and some trace element concentrations.

[26] The fourth problem is the presence of continental erratics [*Paduan et al.*, 2007]. Most of them are easily identifiable based on lithology, size, and rounded shapes but some of the calc-alkaline volcanic erratics are not easily distinguished from hawaiite, even in thin section. Although aware of the problem, we still analyzed six for chemistry (Data Set S2) and Ar-Ar dated 3 of these (Table 1) because they were petrographically so similar to plagioclase-rich hawaiite samples from the seamounts.

4.4. Major Element Compositions

[27] Representative glass and whole-rock compositions are presented in Tables A2 and A3, respectively. Compositions of 48 new dive samples from Pioneer range from alkalic basalt to mugearite, similar to the 8 dive and 4 dredge samples previously reported by *Davis et al.* [2002]. Glass compositions span a comparable range, except some of the mugearite glass compositions from dive T892 have higher alkali contents, and hence plot closer to the basanite/tephrite field (Figure 2), relative to the previous samples. More evolved compositions, like the benmoreite and trachyte found on Davidson [*Castillo et al.*, 2010; *Clague et al.*, 2009b], were not found during the Pioneer dives. On Gumdrop and Guide [*Davis et al.*, 2002], the dominant composition is hawaiite (Figure 2); alkalic basalt and mugearite are less abundant.

[28] Analyses of 103 new samples from Rodriguez greatly expand the compositional range previously reported for the six dredge samples of *Davis et al.* [2002] and the five dredge samples of *Palmer* [1964]. In addition to alkalic basalt and hawaiite, mugearite, benmoreite, and trachyte were also recovered on the dives. Except for the crystal-rich benmoreite and trachyte that had no analyzable glass, glass compositions cover a similar range as the whole-rock samples, but with considerably less scatter. Sulfur in most of the glasses is low (~0.03–0.04 wt %) but in one sample, sulfur contents of >0.09 wt % in a glass inclusion in plagioclase indicates higher initial sulfur and significant degassing (Figure 3). Extensive degassing is consistent with eruption in shallow water.

[29] Of the 49 samples analyzed from Northeast Bank, nearly all whole-rock samples are alkalic basalt with a fairly narrow compositional range, whereas the glass compositions, including the volcaniclastic samples from the R/V *Agassiz* dredge [*Hawkins et al.*, 1971], are all hawaiite (Figure 2). No mugearite, or more evolved volcanics, were recovered. Sulfur contents of glasses are as low as for most of the Rodriguez samples (Figure 3), suggesting eruption in shallow water [*Paduan et al.*, 2009].

[30] The 54 rocks analyzed from the three dives on San Juan (Figure 1) range from mildly alkalic basalt to basanite (Figure 2). Similar to the other seamounts, hawaiite is the predominant composition, especially among the glasses, and only the most evolved glass extends into the mugearite field. Benmoreite and trachyte were not recovered. However, San Juan is the largest of these seamounts and the three dives, although representing different regions and a considerable range of depths, sampled only a small fraction of this huge edifice. Basanite, the only strongly alkalic volcanic rock collected from these seamounts, is present as whole-rock samples, glass rims on pillow fragments, and as glass grains in push core and sediment scoop samples only at San Juan on dive T664 (Table A3). The basanite glass is fresh compared with the other glass samples, consistent with its young Ar-Ar age (2.8 Ma). Although moderately to highly vesicular, the basanite glass still has uniformly high sulfur contents (>0.10 wt %) consistent with eruption in deep water. Based on sulfur in some glass inclusions in minerals, some of the

[1] Auxiliary materials are available at ftp://ftp.agu.org/apend/gc/2010gc003064.

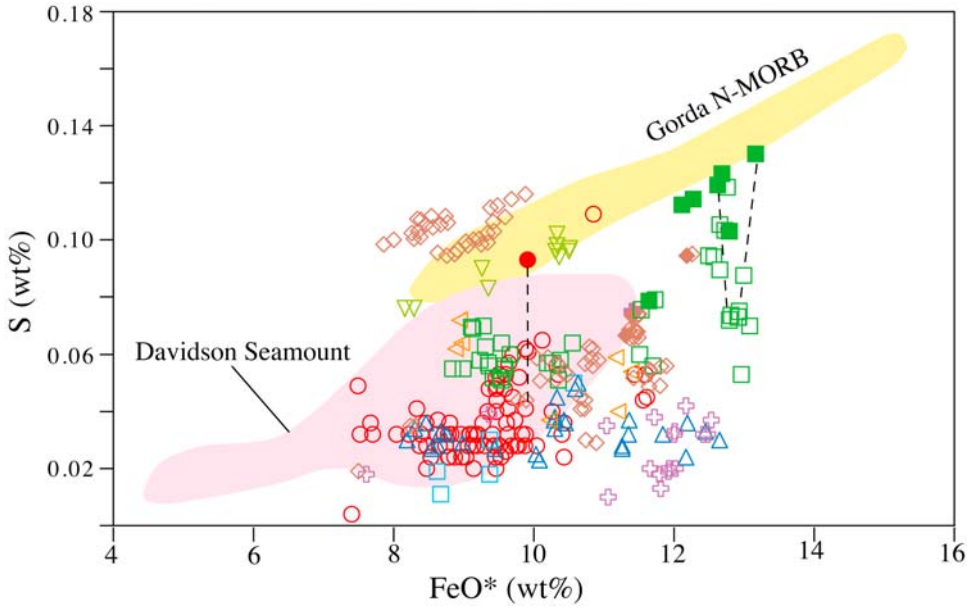

Figure 3. Sulfur versus FeO* in glass shows the basanite from San Juan and the tholeiitic to transitional basalt from Little Joe with sulfur content comparable to MORB from Gorda Ridge. All other samples have degassed to varying extent, as suggested by the sulfur content of glass inclusions in plagioclase (filled symbols). Tie lines connect some glass inclusions in minerals with their host glass. Fields of Davidson and Gorda (MORB) glasses are shown for comparison. Data sources and symbols as in Figure 2 except that open symbols were used for glasses so that overlapping points could be seen.

alkalic basalt and hawaiite glasses are significantly more degassed (Figure 3) although all were collected at depths greater than 1000 m. Low sulfur, along with extensive phosphatization of some samples from the shallowest dive (T665) and other evidence [*Paduan et al.*, 2009] suggest that parts of San Juan may also have been above sea level in the past.

[31] The 26 whole rocks and glasses analyzed from the single dive (T669) on San Marcos have a similar compositional range from alkalic basalt to hawaiite, with the most evolved glass close to the field for mugearite (Figure 2). As on the other seamounts, hawaiite is the most abundant lithology recovered and more evolved volcanics were not found. Sulfur contents in glasses are considerably higher (~0.06 wt %) than for most of the Rodriguez or Northeast Bank glasses, but the higher sulfur (>0.10 wt %) in glass inclusions in minerals (Figure 3) indicates significant degassing.

[32] Samples from dive T668 on Little Joe are mostly alkalic basalt and hawaiite but tholeiitic basalt is also present. The eight whole-rock samples have mm to cm thick rims of glass. Two additional volcaniclastic samples with gravel-sized clasts and one layered hyaloclastite consist of fresh nonvesicular glass with unaltered olivine microphenocrysts. The hyaloclastite, similar in appearance to MORB-hyaloclastite from near-ridge seamounts [e.g., *Batiza and Vanko*, 1984; *Davis and Clague*, 2000; *Smith and Batiza*, 1989], is mildly alkalic basalt, and shapes of the grains, including limu-o-Pele particles, suggest pyroclastic eruptions [*Clague et al.*, 2003, 2009a]. The tholeiitic basalts plot in the MORB field (Figure 2), and, with K_2O ranging from 0.47 to 0.85 wt %, resemble E-MORB. The tholeiitic and alkalic basalt and hawaiite have fresh brown glass with unaltered, euhedral olivine microphenocrysts (±plagioclase), in contrast to most of the plagioclase-rich (±clinopyroxene and altered olivine) alkalic basalt and hawaiite from the other seamounts.

[33] There are similar, although not identical, patterns for the seamounts. The most common lava types erupted at different sites, and at different times at a given site, are alkalic basalt and hawaiite. The rock series forms a chemical continuum, and rock names are somewhat arbitrary for those straddling the field boundaries on the silica versus alkalis plot (Figure 2). Some glass compositions in the volcaniclastic samples match whole-rock compositions from the same site, whereas other glass compositions were not represented among the flow samples. Where whole-rock and glass composition could be determined on the same sample,

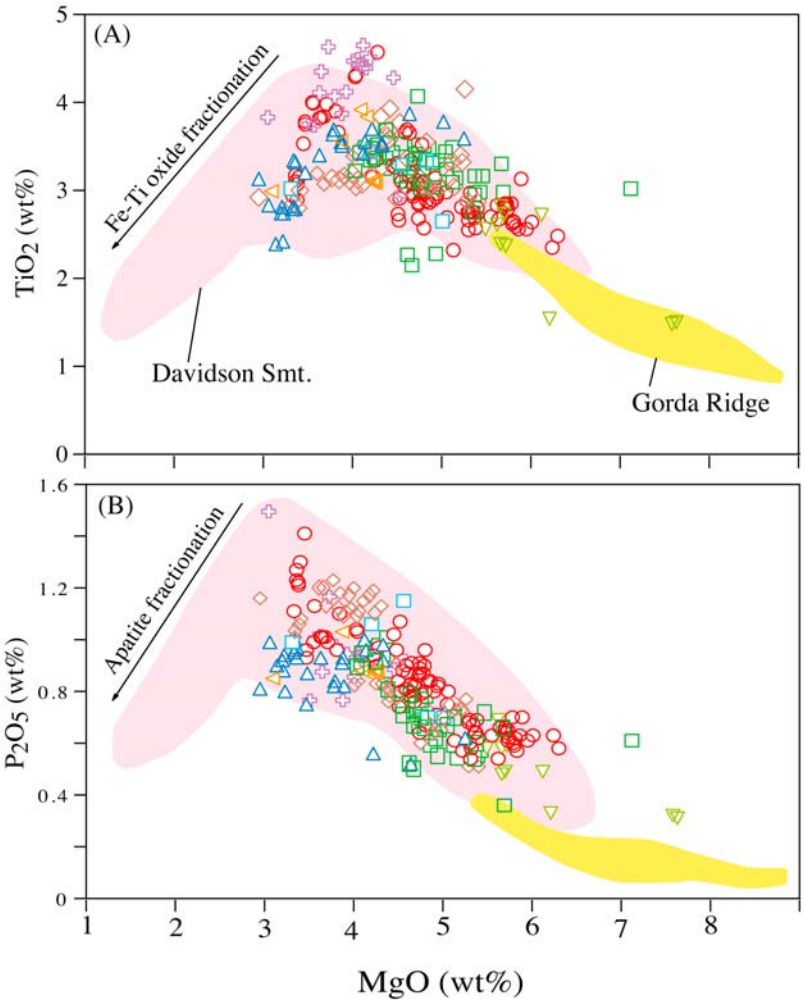

Figure 4. (a) TiO_2 and (b) P_2O_5 versus MgO for seamount glasses show large amount of scatter at comparable MgO content. Crystal fractionation trends of titanomagnetite and apatite are indicated. Fields for Davidson Seamount and Gorda Ridge are again shown for comparison. Data sources and symbols as in Figure 2 except open symbols were used for glasses so that overlapping points could be seen.

the glass composition is typically more evolved (lower MgO, and higher SiO_2) than the bulk rock, reflecting the presence of mafic phenocrysts. The broad spectrum of glass compositions, especially among hawaiite (e.g., Figures 2 and 4), faithfully reflects the chemical diversity of melts erupted at the seamounts. Not all of the seamounts have been sampled as intensively as Davidson and Rodriguez, but highly evolved compositions generally appear to be rare and of small volume. Primitive basalts (>9 wt % MgO) are virtually absent: three olivine-phyric basalts from Northeast Bank have ~9% wt % MgO (Figure 9) and the highest-MgO glass with 8 wt % (Figure 4) is also from there. Tholeiitic basalt and basanite are rare. Both of these rock types are present as whole-rock and fresh glass rinds so the tholeiitic composition cannot result from sodium loss. Similarly, the basanite composition cannot result from addition of alkalis during secondary alteration.

[34] Fractionation trends are typical for alkalic intraplate lavas with TiO_2 increasing with decreasing MgO until about 4 wt % MgO (Figure 4a) and then decreasing when titanomagnetite crystallizes. Typically P_2O_5 is incompatible until about 3% wt % MgO when apatite crystallizes (Figure 4b), as illustrated by the field for Davidson lavas. However, the most evolved glasses from Rodriguez do not include any with <3 wt % MgO. The sulfur contents of the glasses show a large range at a similar FeO* (Figure 3), with the highest values found in Little Joe basalts and San Juan basanites. The high sulfur content of Little Joe basalts and San Juan basanite are similar to North Pacific (Gorda Ridge) MORB. However, many of the

Table 2. Isotopic Compositions of Selected Samples

Sample	$^{87}Sr/^{86}Sr$ (±2σ)	$^{143}Nd/^{144}Nd$ (±2σ)	$^{208}Pb/^{204}Pb$ (±2σ)	$^{207}Pb/^{204}Pb$ (±2σ)	$^{206}Pb/^{204}Pb$ (±2σ)
Pioneer					
T604R7	0.702896 (9)	0.513018 (8)	38.618 (34)	15.555 (13)	19.049 (17)
T627R7	0.702693 (9)	0.513136 (10)	38.343 (2)	15.527 (1)	18.973 (9)
T627R8	0.702757 (12)	0.513123 (8)	38.385 (36)	15.527 (14)	18.981 (20)
Rodriguez					
T628R10	0.703056 (12)	0.512943 (6)	38.816 (20)	15.583 (8)	19.236 (10)
T628R12	0.703037 (10)	0.512967 (8)	38.760 (26)	15.590 (10)	19.259 (12)
T629R15	0.703444 (7)	0.512905 (12)	39.123 (6)	15.641 (3)	19.436 (3)
T629R19	0.703103 (9)	0.512918 (7)	38.793 (2)	15.546 (1)	18.599 (1)
T630R8	0.703094 (11)	0.51290 (14)	38.982 (5)	15.606 (2)	19.377 (2)
T630R12	0.703171 (12)	0.512901 (7)	38.936 (14)	15.613 (7)	19.280 (7)
T631R26	0.703052 (10)	0.512875 (15)	38.703 (9)	15.593 (4)	19.214 (4)
T631R41	0.703154 (6)	0.512902 (22)	38.974 (3)	15.599 (3)	19.409 (4)
T661R16	0.703171 (6)	0.512895 (6)	39.194 (10)	15.641 (4)	19.475 (5)
T661R19	0.703045 (8)	0.512928 (12)	39.031 (3)	15.618 (1)	19.456 (8)
T670R3	0.703098 (16)	0.512926 (3)	39.016 (22)	15.611 (8)	19.461 (9)
T670R18	0.703149 (5)	0.512875 (7)	39.086 (80)	15.621 (30)	19.269 (12)
T670R30	0.703287 (13)	0.512886 (3)	39.054 (9)	15.636 (4)	19.445 (4)
T670R38	0.703522 (20)	0.512871 (3)	39.087 (9)	15.630 (3)	19.423 (2)
San Juan					
T662R8	0.703273 (18)	0.512924 (6)	39.077 (22)	15.632 (9)	19.346 (10)
T664R12	0.703248 (20)	0.513043 (12)	38.491 (14)	15.551 (5)	19.178 (7)
T664R21	0.703152 (11)	0.512922 (14)	38.991 (5)	15.604 (2)	19.362 (3)
T665R22	0.703296 (17)	0.512908 (14)	38.939 (20)	15.592 (15)	19.334 (12)
San Marcos					
T669R2	0.703250 (8)	0.512894 (6)	39.039 (10)	15.619 (3)	19.326 (4)
T669R18	0.703332 (8)	0.512868 (5)	39.039 (10)	15.626 (9)	19.269 (12)
T669R22	0.703174 (6)	0.512943 (6)	38.798 (11)	15.602 (4)	19.185 (5)
Northeast Bank					
T663R22	0.703425 (8)	0.512892 (10)	39.096 (7)	15.636 (2)	19.365 (2)
T663R33	0.703291 (12)	0.512904 (7)	39.111 (7)	15.621 (3)	19.415 (3)
T666R17	0.703199 (8)	0.512923 (5)	39.031 (12)	15.591 (5)	19.338 (6)
T666R31	0.703448 (10)	0.512889 (3)	39.116 (15)	15.652 (6)	19.515 (7)
T666R38	0.703295 (12)	0.512873 (4)	39.052 (12)	15.617 (5)	19.358 (7)
Little Joe					
T668R3	0.703194 (14)	0.512921 (5)	39.055 (9)	15.623 (3)	19.349 (4)
T668R7	0.702917 (12)	0.512922 (4)	38.517 (20)	15.561 (11)	19.029 (14)
T668R17	0.703254 (18)	0.513018 (8)	38.979 (11)	15.617 (4)	19.315 (5)
T668R19	0.703251 (10)	0.512855 (16)	38.854 (14)	15.610 (6)	19.202 (8)

other glasses are degassed to varying degrees, based on the higher S concentrations in glass inclusions in minerals and high vesicularity of the glasses. Northeast Bank samples, many Rodriguez samples, and some San Juan samples are extensively degassed in agreement with other evidence that these seamounts were islands [*Paduan et al.*, 2009]. Low sulfur contents for some glasses from Pioneer and Guide suggest some eruptions at these sites also have been in shallow water or subaerial.

4.5. Trace Element Compositions

[35] Trace element compositions of whole rock samples are presented in Table 2 because glasses were not voluminous enough to separate for trace element analyses. We focus primarily on the concentrations of rare earth elements (REE) and high field strength elements (HFSE: Zr, Nb, Ta, Hf, Th, Y) that tend to be resistant to secondary alteration. Phosphatized samples (Data Set S1) are not included in the chemistry plots. Even the most phosphatized samples do not have unusual REE profiles or abnormal HFSE element abundances.

[36] The HFSE and REE elements show less scatter (Figures 5 and 6) than the major elements (Figures 2–4). Zr and Nb (Figure 5a) have a well-defined positive correlation and the Zr/Nb ratios are typical of alkalic lavas, even for the samples that plot in the MORB field on the alkali versus silica plot (Figure 2). Zr/Nb ratios range from ~6 to 3, with the basanite from San Juan having the lowest ratio. Th versus Hf (Figure 5b)

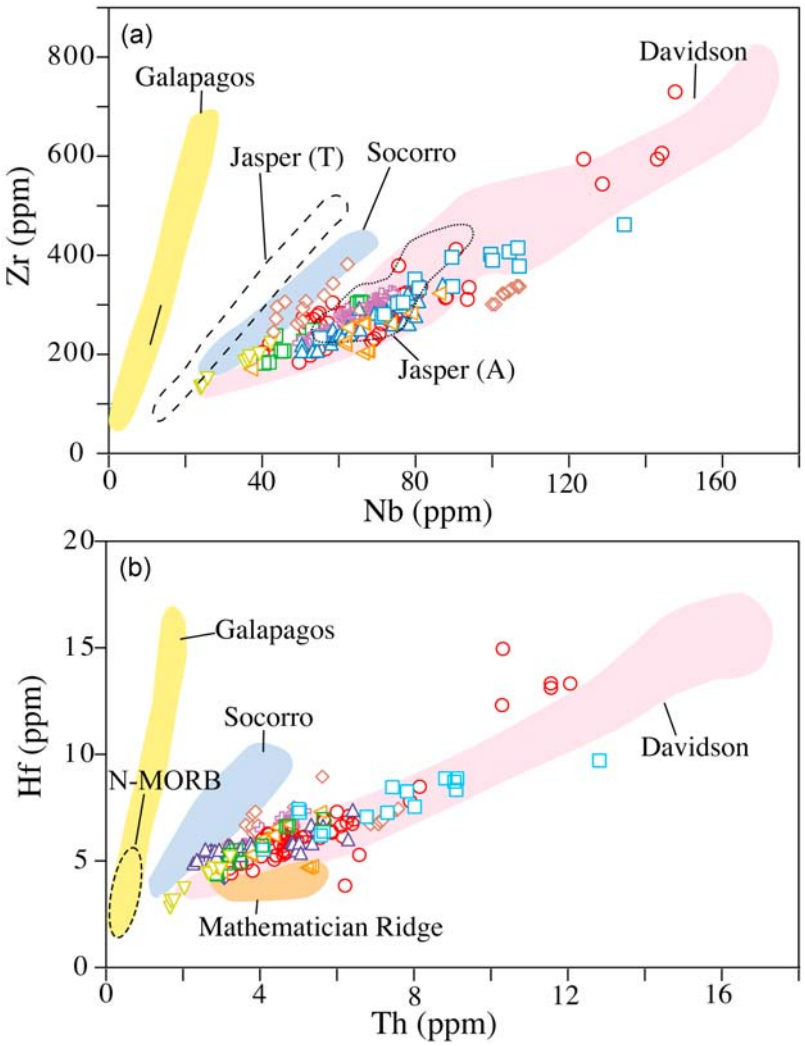

Figure 5. (a) Zr versus Nb and (b) Hf versus Th for whole-rock samples from the seamounts have abundances and ratios typical for alkalic ocean island basalt (OIB). Jasper (A) are summit alkalic lavas from *Gee et al.* [1991]. Davidson lavas [*Castillo et al.*, 2010; *Davis et al.*, 2002] have as large a range of compositions as all of these eight seamounts combined. Compositions from the Mathematician Ridge [*Batiza and Vanko*, 1985] overlap with those from the seamounts but are at the less fractionated end. Basalts from Socorro [*Bohrson and Reid*, 1995], similar to the transitional basalts (T) from the flanks of Jasper [*Gee et al.*, 1991], are closer to the MORB trend. Symbols as in Figure 2. Data for Galapagos fractionation trend from *Perfit et al.* [1983].

and Ba versus La, show similar trends with the least alkalic compositions approaching the field for N-MORB. The chondrite-normalized REE have high light to heavy (LREE/HREE) ratios (Figure 6) typical of alkalic compositions, with the basanite having the steepest profile and lowest HREE abundances. The tholeiitic basalts from Little Joe also have LREE-enriched profiles although they are less steep and overall abundances are lower. The most evolved volcanics have the highest REE abundances with profiles that are parallel to some of the hawaiites. At each site, samples have chondrite-normalized REE profiles that crosscut each other, whether the seamount is located on the Pacific plate or within the continental margin.

4.6. Isotopic Compositions

[37] Sr, Nd, and Pb isotopic compositions of 33 samples are given in Table 2. Collectively, the seamount samples have a large range in radiogenic isotopes. The new $^{87}Sr/^{86}Sr$ ratios (Figure 7a) do not include any >0.704 as some previously published for Rodriguez and San Marcos [*Davis et al.* 1995], but these earlier samples were less severely acid-leached and may have been contaminated by seawater alteration. In agreement with previous data,

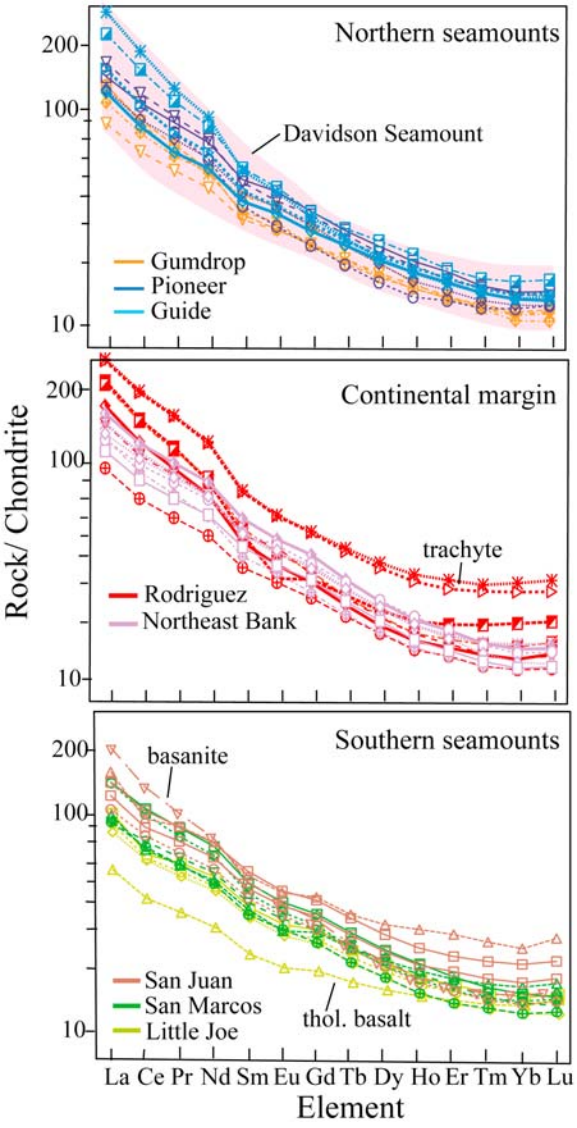

Figure 6. Chondrite-normalized REE for whole-rock samples have LREE-enriched profiles typical of alkalic basalts, even for the tholeiitic and transitional basalts from Little Joe, although they have lower abundances. The patterns are similar whether the seamount resides on the Pacific plate, at the continental margin, or within the Continental Borderland. Normalizing values from *Sun and McDonough* [1989].

new $^{87}Sr/^{86}Sr$ analyses of Pioneer and Gumdrop samples plot in the Pacific MORB field [*Davis et al.*, 2002]. The basanite and one tholeiitic (T668R7) basalt from Little Joe also plot near the MORB field whereas all other samples are similar to other alkalic ocean island basalts (OIB) in the Pacific Ocean. Davidson, even more extensively sampled than these seamounts, has as broad a range of isotopic compositions [*Castillo et al.*, 2010] as all of these seamounts combined (Figure 7). $^{143}Nd/^{144}Nd$ and Pb isotopes, less susceptible to seawater alteration, show less scatter than Sr isotopes, although they also show a considerable range. Pb isotopic compositions are at the more radiogenic end of the MORB spectrum (Figures 7b and 7c), and overlap with compositions from seamounts near the East Pacific Rise with respect to $^{208}Pb/^{204}Pb$ [*Graham et al.*, 1988; *Zindler et al.*, 1984].

5. Discussion

5.1. Ages Relative to Tectonic Setting

[38] The structurally similar, northeast-southwest trending seamounts scattered along the continental margin from central California to Baja, Mexico, represent an unusual type of intraplate oceanic volcanism related to rotation and abandonment of ridge segments when the plate boundary shifted from subduction to a transform regime. Only Davidson and Guide and Guadalupe Island have symmetrically distributed magnetic anomalies thus identifying them as atop fossil spreading ridges [*Atwater and Severinghaus*, 1989; *Lonsdale*, 1991; *Castillo et al.*, 2010]. However, identification of anomalies may not be conclusive because of the presence, rotation, and partial subduction of numerous small microplates [e.g., *Atwater*, 1989; *Lonsdale*, 1991; *Nicholson et al.*, 1994]. The multiple, aligned, parallel ridges and troughs shared by all the seamounts appear to reflect the underlying ocean crust fabric. Seafloor spreading ceased at Davidson at about 20 Ma, but the oldest dated lava erupted at least 5 million years later [*Clague et al.*, 2009b] because the 16 Ma old basaltic andesite from Davidson [*Davis et al.*, 2002] is now interpreted to be a calc-alkaline erratic unrelated to the construction of the seamount [*Clague et al.*, 2009b]. At each of the dated seamounts, lavas are younger than the underlying ocean crust by 4 to 11 million years (Figure 8). A similar pattern has been reported for Guadalupe Island off Mexico, where seafloor spreading ceased at about 12 Ma but the oldest dated lavas are about 5.4 ± 0.8 Ma [*Batiza et al.*, 1979]. Lavas too young to date indicate volcanic eruptions also occurred in recent times [*Batiza*, 1977a]. Farther south, Socorro Island is built on top of a spreading center that was abandoned at about 3.5 Ma when spreading shifted to the East Pacific Rise. Silicic caldera forming eruptions on Socorro are dated at 540 to 370 ka, followed by basaltic volcanism from about 150 to 70 ka [*Bohrson et al.*, 1996]. A basaltic submarine eruption was reported in 1993 [*Bohrson et al.*, 1996; *Siebe et al.*, 1995] indicating that episodic eruptions continue.

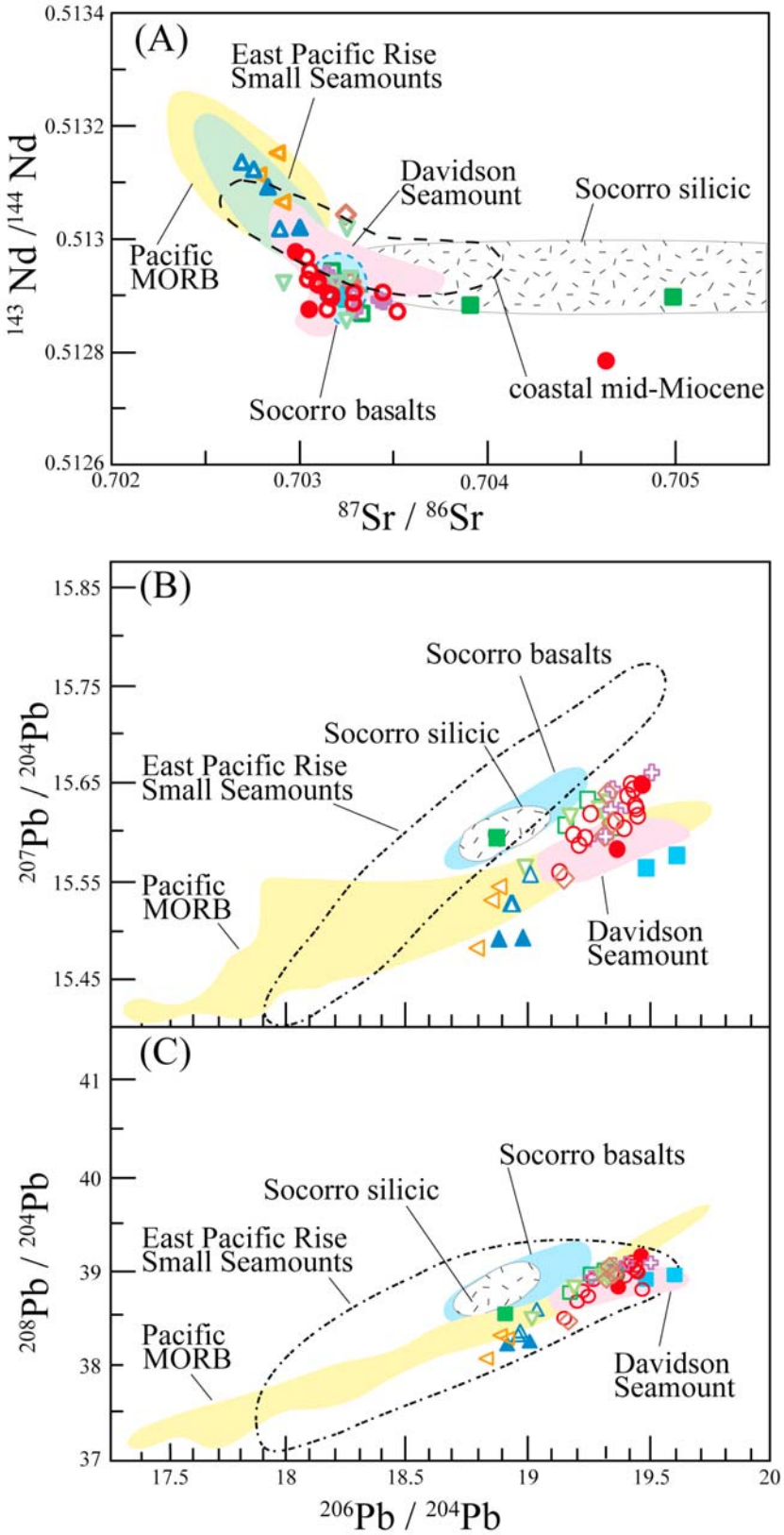
(A)
East Pacific Rise
Small Seamounts
Davidson
Seamount
Socorro silicic
Pacific
MORB
coastal mid-Miocene
Socorro basalts
0.5134
0.5132
0.513
0.5128
0.5126
0.702
0.703
0.704
0.705
143 Nd /144 Nd
87Sr / 86Sr
(B)
Socorro basalts
Socorro silicic
East Pacific Rise
Small Seamounts
Pacific
MORB
Davidson
Seamount
15.85
15.75
15.65
15.55
15.45
207Pb / 204Pb
(C)
Socorro basalts
Socorro silicic
East Pacific Rise
Small Seamounts
Pacific
MORB
Davidson
Seamount
41
40
39
38
37
17.5
18
18.5
19
19.5
20
208Pb / 204Pb
206Pb / 204Pb

Figure 7

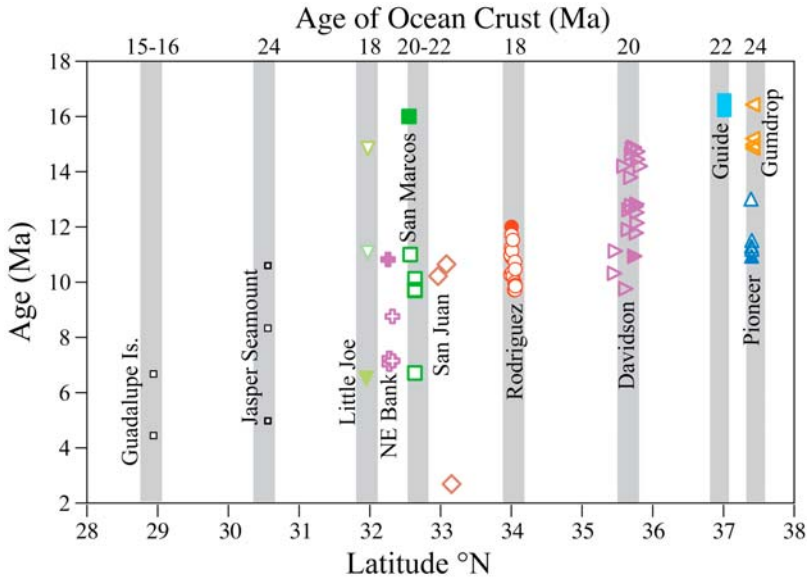

Figure 8. Age versus latitude plot for the volcanoes offshore California to Baja indicates multiple episodes of volcanism that are roughly synchronous at widely separated locations. Although a considerable range of ages is found on numerous seamounts, in a general way volcanism appears to get younger southward. Previously published ages for some of the same seamounts [*Bohrson and Davis*, 1994; *Davis et al.*, 1995, 2002] are indicated by filled symbols. New ages for Davidson from *Clague et al.* [2009b]. Data for Jasper from *Pringle et al.* [1991] and for Guadalupe Island from *Batiza et al.* [1979].

[39] The seamounts are morphologically different from classical hot spot volcanoes like the Hawaiian chain and they do not form age progressive chains. Also, unlike Hawaiian volcanoes that build a large-volume edifice of tholeiitic basalt in a million years or less, the seamounts are built by small eruptions, mostly of hawaiite, over periods spanning millions of years. Although each seamount does not follow the same age pattern, ranges for volcanism as long as 5 to 8 Myr for Davidson [*Clague et al.*, 2009b] and San Juan, respectively, are now documented. Ages reported for Jasper in the Fieberling-Guadalupe chain also span 7 Myr [*Pringle et al.*, 1991] and the oldest volcanism is roughly coeval with ages determined for all the seamounts at the continental margin (Figure 8). Collectively, the age pattern for these seamounts shows that the most widespread, and probably most voluminous, volcanism occurred between 7 and 16 Ma, probably due to crustal extension at the continental margin related to trans-tensional tectonics. The surprisingly young age of 2.8 Ma at San Juan suggests that some of these volcanoes may be dormant but not extinct. Although coeval episodes of volcanism occurred at multiple sites, generally volcanism appears to get younger southward (Figure 8). The intersection of spreading centers with the continental margin also progresses from north to south [e.g., *Atwater*, 1970, 1989;

Figure 7. Isotopic compositions of whole-rock samples from the seamounts. (a) Plot of $^{87}Sr/^{86}Sr$ versus $^{143}Nd/^{144}Nd$ shows some from the northern sites and the tholeiitic basalt from Little Joe as well as the basanite from San Juan in or near the MORB field. The other samples are more radiogenic. Filled symbols are previously published analyses of *Davis et al.* [1995, 2002] that were not as severely acid-leached and include three samples with higher $^{87}Sr/^{86}Sr$ values. Compositions from Davidson Seamount [*Castillo et al.*, 2010] span a similar but slightly smaller range. Likewise, mid-Miocene coastal basalts [*Cole and Basu*, 1995] have a similar range but include some higher $^{87}Sr/^{86}Sr$ values. Basalts from Socorro Island have a much more restricted range, whereas the Socorro silicic compositions have an enormous range in $^{87}Sr/^{86}Sr$ [*Bohrson and Reid*, 1995, 1997], which has been attributed to assimilation of altered ocean crust. Plots of (b) $^{207}Pb/^{204}Pb$ and (c) $^{208}Pb/^{204}Pb$ versus $^{206}Pb/^{204}Pb$ show the seamounts at the more radiogenic end of the MORB spectrum. Both Davidson and Socorro have narrower ranges of Pb isotopic compositions than the seamounts. Pacific MORB field from *White et al.* [1987], *Castillo et al.* [2000, and references therein], and *Church and Tatsumoto* [1975] and East Pacific Rise seamounts from *Graham et al.* [1988] and *Zindler et al.* [1984].

Lonsdale, 1991], suggesting that the two are related phenomena.

5.2. Formation of Seamount Lavas

[40] The most distinctive feature of the seamount lavas is that they primarily consist of alkalic basalt to hawaiite (Figure 2) independent of their location on the Pacific plate or at, or within, the continental margin. The petrogenesis of these lavas is, therefore, very similar to that for Davidson, and is discussed in detail by *Castillo et al.* [2010]. At a given seamount, hawaiite erupted at different locations and at different times, in some cases millions of years apart. Major element trends are consistent with fractional crystallization but from slightly different isolated reservoirs of parental magmas located near the mantle-crust boundary [*Davis et al.*, 2007]. Primitive (>8 wt % MgO) melts that could be parental to the generally low-MgO alkalic basalts and hawaiites are absent; the most magnesian whole-rock compositions are altered, and may contain accumulated olivine and thus are questionable as parental magmas. However, liquid lines of descent determined with the MELTS program [*Ghiorso and Sack*, 1995] for a similar, but more complete range of lava compositions from Davidson indicate that the lavas cannot be related by simple crystal fractionation at a given pressure [*Davis et al.*, 2007].

[41] Experimental data for crystallization of alkalic lavas have shown that the fractionation assemblages are strongly pressure sensitive [*Nekvasil et al.*, 2004]. Clinopyroxene is a prominent early phase at higher pressure [e.g., *Mahood and Baker*, 1986; *Nekvasil et al.*, 2004] in contrast to olivine-plagioclase dominated assemblages at lower pressure. The nearly constant CaO/Al_2O_3 (Figure 9a) and Sc (Figure 9b) with decreasing MgO are consistent with multiphase crystal fractionation involving clinopyroxene and plagioclase at variable but moderate pressures for most of the seamount lavas. The exception is the tholeiitic and transitional basalts from Little Joe that have higher CaO/Al_2O_3 that increases with decreasing MgO and have the plagioclase-olivine dominated fractionation trend typical for MORB. *Nekvasil et al.* [2004] pointed out that tholeiitic and transitional basalt compositions do not require significantly different sources but can be generated from similar parental melts at different depths. An origin by crystal fractionation from a common parent but at different depths has been proposed for spatially closely related alkalic and tholeiitic basalt in the Galapagos Islands [*Naumann and Geist*, 1999], and this is consistent with nearly identical ratios of highly incompatible elements (e.g., Zr/Nb, Ba/La, La/Yb). However, the seamount volcanics have variable trace element ratios of highly incompatible elements and isotopic ratios suggesting small-scale mantle source heterogeneity.

[42] Most likely, crystallization occurred initially at or below the crust-mantle boundary, followed by minor crystallization as the lavas ascended. Mineral chemistry of xenoliths, phenocrysts, and microlites in Davidson lavas is compatible with polybaric fractionation [*Davis et al.*, 2007]. Plagioclase crystals in the Davidson lavas are sodic, consistent with experimental studies that show that plagioclase is more sodic at higher pressures [e.g., *Bender et al.*, 1978; *Mahood and Baker*, 1986; *Nekvasil et al.*, 2004].

[43] The presence and partial dissolution of alkalic gabbro xenoliths from the margins of the magma reservoir may add an additional complexity to the seamount lavas. Xenoliths of amphibole-biotite gabbro, as found in Davidson lavas, are partially disaggregated and have ubiquitous melt reaction rims and rounded amphibole megacrysts providing evidence for some melt-rock interactions [*Davis et al.*, 2007].

[44] Not every seamount has been as intensively sampled as Rodriguez and Davidson or is represented by their range of chemical compositions. However, collectively the seamount lavas show a similar compositional and evolutionary pattern. Based on the large number and wide distribution of samples collected, the main edifices of these seamounts appear to be constructed mainly from many small eruptions of hawaiite and low-MgO alkalic basalt that occurred repeatedly over a long period of time. The general trend of transitional or tholeiitic early lavas to most strongly alkalic late lavas seen in both Hawaii [*Clague and Dalrymple*, 1987] and at Jasper [*Konter et al.*, 2009] is poorly represented at the seamounts studied here. However, the most alkalic lava, a basanite from San Juan, is also the youngest dated lava, and transitional or tholeiitic lavas occur at Davidson [*Clague et al.*, 2009b] and Little Joe, although we do not know when they erupted during the growth of the volcanoes. For this type of seamount built on or near abandoned spreading centers, such chemically early and late lavas appear to be rare and could remain unknown with less intensive sampling than we have done.

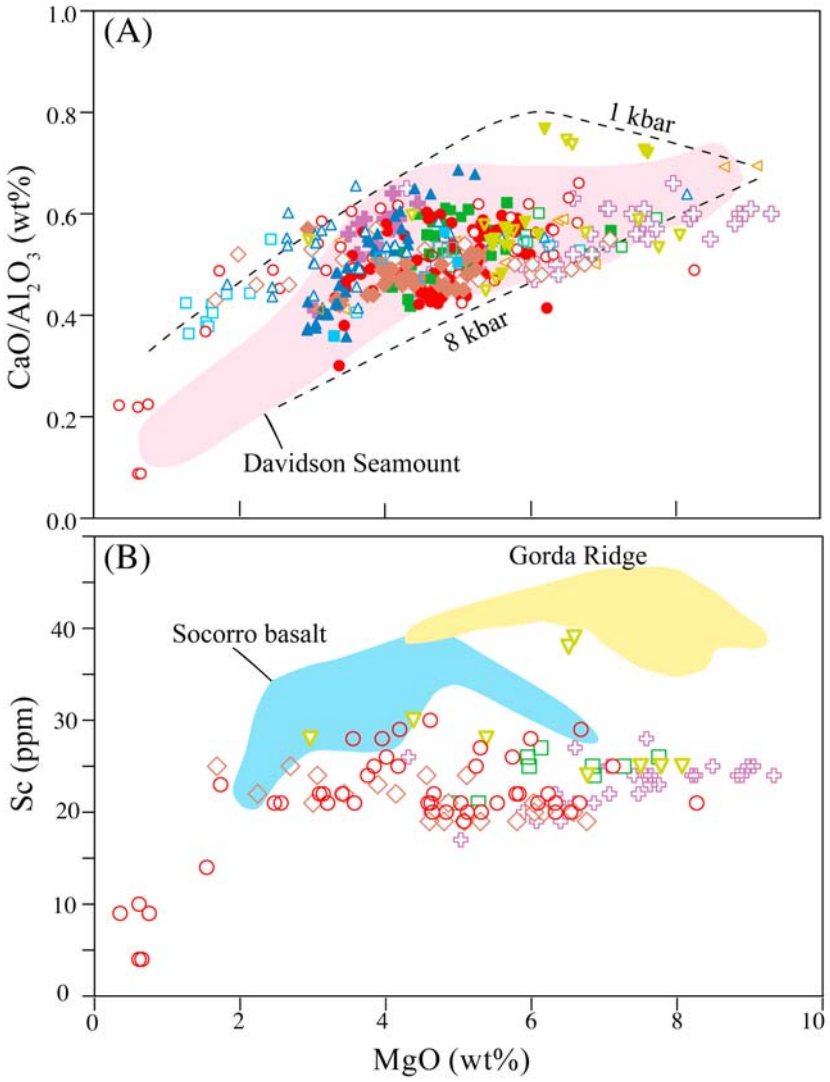

Figure 9. (a) CaO/Al_2O_3 versus MgO for seamount lavas shows large amount of scatter, especially for the hawaiite, compatible with fractionation over a range of depths. Calculated liquid lines of descent [*Ghiorso and Sack*, 1995] at 1 kbar and 8 kbar are indicated. Field for Davidson Seamount shows a similar pattern. (b) Sc versus MgO shows a narrower trend because Sc is only compatible in clinopyroxene over this compositional range. The trend shown by Socorro basalts is closer to that of MORB. Symbols and data sources as in Figure 2.

5.3. Comparison With Seamounts Built on Known Abandoned Spreading Centers

[45] The similarity in morphology, chemistry, and age distribution of these seamount lavas with those from Davidson [*Clague et al.*, 2009b; *Castillo et al.*, 2010] suggests that they are all related in origin. Continental margin volcanoes owe their origin to abandonment and partial subduction of spreading ridge segments and oceanic microplates when the tectonic regime changed to a transform margin [e.g., *Atwater and Severinghaus*, 1989; *Dickinson*, 1997; *Lonsdale*, 1991; *Nicholson et al.*, 1994]. Small spreading ridge segments may have been overridden by the continental margin and thus underlie Rodriguez and Northeast Bank. However, most of northeast-southwest alignment of seamounts may principally reflect zones of weakness provided by the ridge-parallel structure of the subducting oceanic plate.

[46] Volcanoes built on top of known abandoned spreading centers like Socorro Island [*Bohrson and Reid*, 1995], Guadalupe Island [*Batiza*, 1977a, 1977b], and the Mathematician Ridge [*Batiza and Vanko*, 1985], have major and trace element abundances and ratios that are typical of alkalic ocean islands. This also is the case for the seamounts described here; the volcanics are clearly alkalic and do not have MORB affinities. Most of the sea-

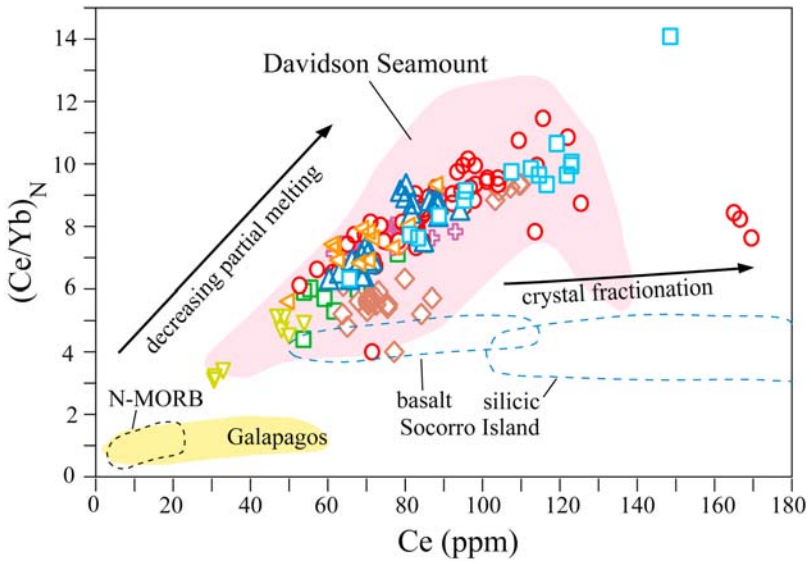

Figure 10. Chondrite-normalized Ce/Yb versus Ce abundance shows trends compatible with varying degrees of partial melting of somewhat variable sources. Davidson lavas show a similar pattern. In contrast, basalt and silicic compositions from Socorro Island appear primarily controlled by crystal fractionation processes. Data sources as in Figure 2.

mounts have Zr/Nb (Figure 5) that are intermediate between the least alkalic samples from Little Joe (~6) and the most alkalic basanite from San Juan (~3 (Figure 2)).

[47] A similar pattern was observed on Jasper with the less alkalic lavas, referred to as the flank transitional series by *Gee et al.* [1991], having a narrow range of higher Zr/Nb ratios compared to the younger, more variable alkalic series volcanics collected from the summit. Basalts from Socorro have a narrow range in Zr/Nb (6.3 ± 0.5), similar to those from San Juan and the Jasper flank transitional basalts, and are closer to the MORB trend. A comparable pattern is shown with Th versus Hf (Figure 5b); the Socorro basalts having high Hf/Th are closer to the MORB trend whereas basalts from the Mathematician Ridge [*Batiza and Vanko*, 1985] have lower Hf/Th than the seamount lavas. Chondrite-normalized Ce/Yb ratios are not significantly affected by crystal fractionation at low pressure but are sensitive to degree of partial melting, source composition, or high-pressure crystal fractionation with abundant clinopyroxene. The seamount lavas show a large range in $(Ce/Yb)_N$ (Figure 10) compatible with variations in degree of partial melting or variable source composition. In contrast, Socorro basalts have a narrow range of lower $(Ce/Yb)_N$ indicating a similar degree of partial melting but larger than for most of the seamount lavas. Apparently, extensive crystal fractionation was a more important process for the Socorro basalts [*Bohrson and Reid*, 1995] and it probably occurred at shallower depth involving less, or later crystallization of clinopyroxene (Figure 9). At Socorro the basalts were predated by eruption of large volumes of caldera-forming silicic peralkaline lavas that were stored in shallow magma reservoirs and reacted with altered ocean crust [*Bohrson and Reid*, 1997]. In contrast, highly evolved compositions from Rodriguez and Davidson [*Castillo et al.*, 2010; *Clague et al.*, 2009b] are of small volume and found only as small isolated cones. The absence of calderas and pit craters on all of these seamounts is consistent with a lack of shallow storage reservoirs within the volcanic edifices.

[48] The variations in isotopic composition indicate variable source compositions (Figure 7), with a range similar to that previously reported by *Davis et al.* [2002] except that one of their two dredge samples from Rodriguez had unusually high $^{87}Sr/^{86}Sr$ without a correspondingly lower $^{143}Nd/^{144}Nd$ (Figure 7a). Two glass samples dredged from San Marcos had similar high $^{87}Sr/^{86}Sr$ at moderate Nd isotopic ratios [*Davis et al.*, 1995]. Sr isotope compositions are highly sensitive to seawater alteration, and acid leaching of the samples has been shown to significantly reduce the $^{87}Sr/^{86}Sr$ [*Bohrson and Reid*, 1995; *Castillo et al.*, 2010]. All of our new analyses are of severely acid-leached samples and none have the exceptionally high $^{87}Sr/^{86}Sr$ seen previously. The pattern shown by the Nd and Pb isotope compositions is similar,

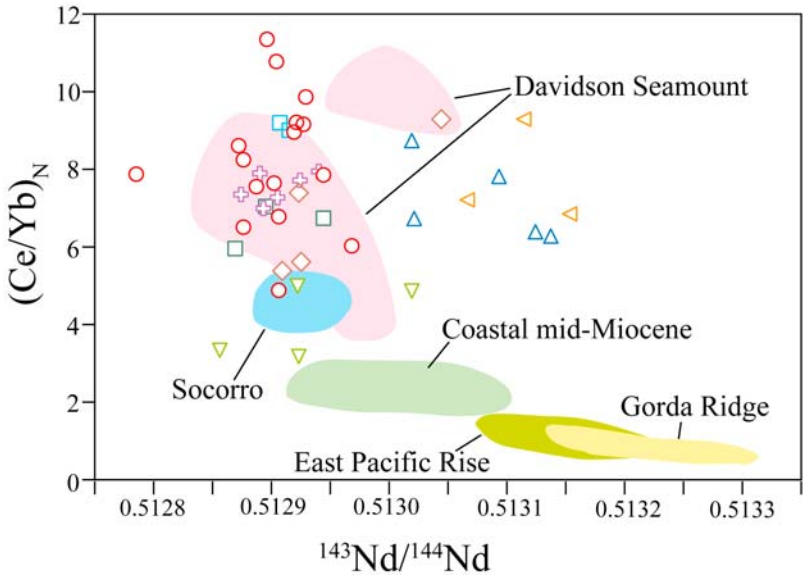

Figure 11. Chondrite-normalized Ce/Yb versus $^{143}Nd/^{144}Nd$ shows just how much more variable with respect to degree of partial melting and source heterogeneity the seamount lavas are compared with Socorro basalts [*Bohrson and Reid*, 1995]. Some of the mid-Miocene basalts erupted in coastal California [*Cole and Basu*, 1995] are closer to the MORB field.

indicating less radiogenic sources for the northern sites and the tholeiitic and basanite samples (Figure 7). The entire range of seamount isotopic compositions is considerably larger than for Socorro or the Mathematician Ridge suggesting more variable mantle sources beneath this large region. The large scatter in $(Ce/Yb)_N$ versus $^{143}Nd/^{144}Nd$ (Figure 11) shows how much more variable the seamount lavas are both in degree of melting and source enrichments relative to basalts from Socorro Island. Although there is no clear correlation between age and chemistry, the basanite from San Juan is by far the youngest, suggesting that lavas may get more alkalic with younger age. Such a relationship would be expected when magmas originate at greater depths as the ocean lithosphere cools and thickens. On the other hand, the only dated transitional basalt from Davidson [*Clague et al.*, 2009b] is not one of the oldest dated samples.

5.4. Model for Volcanism for the Continental Margin Volcanoes

[49] Despite considerable diversity in ages and chemistry, there is a pattern of volcanism for these seamount lavas and those demonstrated to be built on abandoned spreading centers that forms a continuation of the N- and E-MORB fields (Figures 12 and 13). As spreading rate decreases, degree of partial melting also generally decreases and the enriched components, ubiquitous in the suboceanic mantle, form a larger proportion of the resultant melt and thus lavas tend to evolve toward enriched compositions [e.g., *Davis et al.*, 1998, 2008; *Haase et al.*, 1996, 2003]. At ultraslow spreading ridges E-MORB becomes a common composition [e.g., *Mühe et al.*, 1997; *Haase et al.*, 1996, 2003; *Hellebrand et al.*, 2001] compared to the more common N-MORB at faster spreading ridges.

[50] Mantle upwelling slows when the spreading center is abandoned and decompression melting produces only small melt volumes derived from the most enriched mantle components. The composition and volume of melt generated may largely be controlled by the amount and distribution of enriched components in the suboceanic mantle. The enriched components may consist of veins, pods, and layers, possibly of pyroxenite, with a lower melting point than the surrounding lherzolite matrix [e.g., *Niu et al.*, 1999]. At a recently abandoned spreading center, such as at Socorro Island, the ocean crust is thin and the melt may pond and extensively fractionate at shallow depth. As time goes by, as represented by the growth of these seamounts, the oceanic lithosphere thickened and melts formed at progressively greater depths, generally becoming more alkalic as degree of melting decreased and clinopyroxene became an earlier fractionating phase.

[51] The kind and amount of melt generated may depend on the enriched, and more easily melted

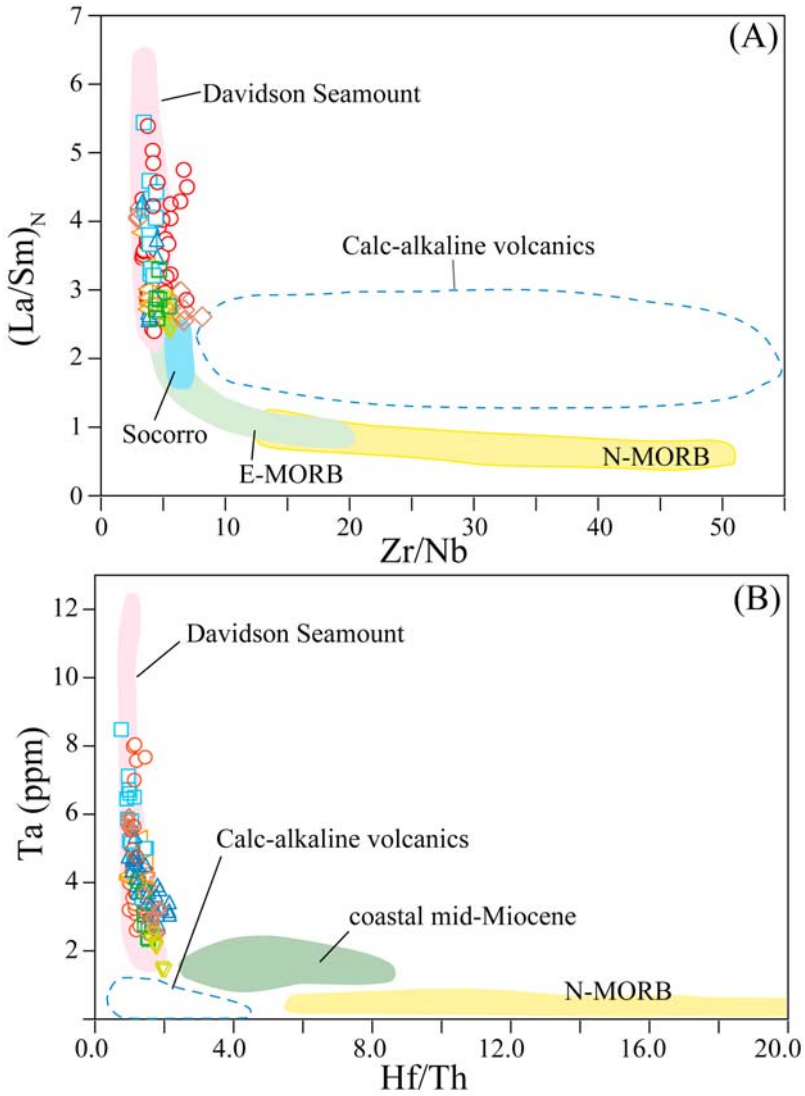

Figure 12. (a) Chondrite-normalized La/Sm versus Zr/Nb shows a continuous trend from N- to E-MORB and to the seamounts in LREE enrichment as well as in Nb, which results in higher Zr/Nb ratios. Socorro basalts are at the less enriched end, overlapping with E-MORB. (b) Ta versus Hf/Th show a similar pattern, but the mid-Miocene basalts, which erupted presumably through a "slab window," have compositions overlapping with N-MORB. Compositions of calc-alkaline erratics (Data Set S2) and onshore volcanics [*Weigand et al.*, 2002] have distinctively lower Nb and Ta, characteristic of subduction-related lavas. Data sources as in Figure 11.

component in the mantle, which may also determine if postspreading magmatism would occur instead of amagmatic rifting. The similar level of differentiation at different sites and eruption times suggests a repetitive process with seamount magmas fractionating extensively during prolonged storage, probably near the crust/mantle boundary. The high volatile content of the melts, as evidenced by amphibole and biotite in the alkalic cumulate xenoliths on Davidson [*Davis et al.*, 2007], may provide the driving force necessary to propel small batches of these relatively viscous lavas to the seafloor. As the crust cools, the process may be aided by, or even require, the presence of lithospheric fractures and transtensional tectonics related to fault movement along the continental margin [e.g., *Cole and Basu*, 1992, 1995; *Davis et al.*, 1995, 2002; *Dickinson*, 1997; *Weigand et al.*, 2002]. Extensional tectonics helping small batches of magma to erupt has also been proposed by *Batiza and Vanko* [1985] for the Mathematician Ridge.

5.5. Connection With Volcanism Onshore

[52] Multiple episodes of mid-Tertiary volcanism occurred in widely separated areas of coastal

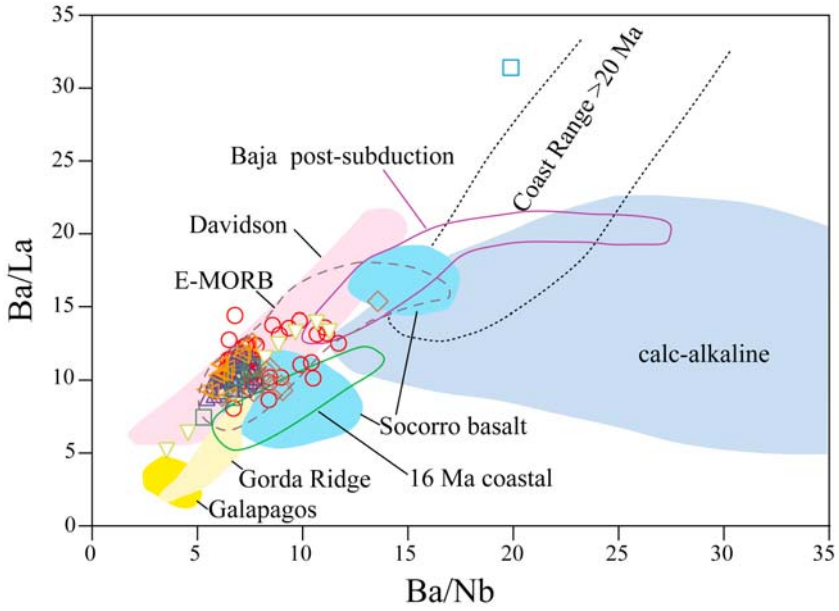

Figure 13. Ba/La versus Ba/Nb shows a trend from N-MORB (represented by Gorda Ridge) to E-MORB that is similar to that shown by the seamounts. Mid-Miocene basalts with MORB-like isotopic signatures [*Cole and Basu*, 1995] plot on the same trend. However, calc-alkaline lavas, including the mid-Miocene Conejo volcanics [*Weigand et al.*, 2002], and analyzed erratics (Data Set S2) plot off that trend with a large and enormously variable range of Ba/La (to >100). The older Coast Range basalts (>22 Ma [*Cole and Basu*, 1995]) as well as the postsubduction lavas in Baja [*Benoit et al.*, 2002] include samples from both groups.

California that, like the seamounts, ultimately owe their origin to the changes that occurred when the boundary between the Pacific and North American plate changed to a transform margin. Although high-precision radiometric ages are sparse or absent for many units in coastal California, several distinct volcanic episodes are indicated at about 22 to 26 Ma, 14 to 16 Ma, and a less well documented episode at about 12 to 10 Ma [*Cole and Basu*, 1992, 1995; *Dickinson*, 1997; *Weigand et al.*, 2002, and references therein]. Most of the lavas erupted, especially the older ones, are calc-alkaline, ranging from basalts to rhyolites with typical subduction-related chemical imprints (Figure 13) [*Cole and Basu*, 1992, 1995; *Weigand et al.*, 2002]. However, middle Miocene basalts with MORB-like isotopic and trace element compositions (Figures 7, 11, 12b, and 13) [*Cole and Basu*, 1992, 1995] occur in close proximity to those with a subduction signature. The continuation of subduction until about 19 Ma [e.g., *Atwater*, 1989; *Lonsdale*, 1991] can explain the older calc-alkaline volcanic units. However, the postsubduction volcanism has been explained as a product of asthenospheric upwelling through "slab windows" in the oceanic plate that was subducted beneath the continental margin [e.g., *Cole and Basu*, 1995; *Dickinson*, 1997; *Weigand et al.*, 2002]. Decompression melting during asthenospheric upwelling resulted in discrete volcanic pulses, where some show the chemical imprint of the descending slab whereas others have a more depleted MORB-like mantle source (fields in Figures 7 and 11–13). Because tectonic models of the plate margin changes involve numerous microplates [*Atwater*, 1989; *Atwater and Severinghaus*, 1989; *Lonsdale*, 1991; *Nicholson et al.*, 1994], formation of slab windows could be a highly complex process. Further complexity can be introduced by contamination with continental crust, especially for the more evolved compositions within the borderland (e.g., Catalina Schist, as proposed by *Weigand et al.* [2002]).

[53] A similar chemical diversity of spatially and temporally related mid-Miocene to Recent, arc-related magmatism in Baja California, Mexico [*Benoit et al.*, 2002] also has been linked to the opening of a slab window following ridge subduction. Among their mostly calc-alkaline and minor tholeiitic basalts are some alkalic basalts (Figure 13), referred to as niobium-rich, which closely resemble the seamount lavas. *Benoit et al.* [2002] proposed three different magma sources, with the niobium-rich basalts produced by melting mantle that was metasomatized by slab-derived melts. In this model, vastly different sources can be tapped at geographically closely related areas and at similar and/or different times, but the sources differ from that

Table A1 (Sample). Summary of Seamount Dive Samples, Locations, and Descriptions[a] [The full Table A1 is available in the HTML version of this article]

Sample	Latitude (°N)	Longitude (°W)	Depth (m)	Analyses	Rock Type	Comment[b]
Gumdrop						
T88R1	37.456	123.459	1562	wr, I	AB	ref 1
T88R3	37.457	123.458	1483	wr	AB	ref 1
T88R7	37.452	123.457	1436	wr	AB	ref 1
T88R8	37.451	123.457	1424	wr	AB	ref 1
T88R9	37.449	123.456	1408	wr, I	AB	ref 1
T88R10	37.447	123.458	1478	wr, I	AB	ref 1
T122R2	37.414	123.460	1920	wr, A	AB	ref 1
T122R5	37.416	123.463	1925	wr, gr, A	Haw	
T122R6	37.415	123.463	1925	gr	Haw	ref 1
T122R9	37.414	123.463	1921	wr, gr, A	Haw	
T122R14	37.417	123.464	2023	wr, gr	Haw	ref 1
T122R15	37.418	123.465	2031	wr	Haw	ref 1
T122R19	37.423	123.469	1847	wr, A	Haw	
Guide						
T90R2	36.987	123.374	1847	wr	Mug	ref 1
T123R1	36.938	123.382	2717	wr	AB	ref 1
T123R9	36.941	123.384	2726	wr	Mug	ref 1
T123R10	36.947	123.385	2717	wr	AB	ref 1
T123R11	36.947	123.384	2717	wr	Mug	ref 1
T123R12	36.948	123.383	2728	wr	Haw	ref 1
T123R13	36.946	123.384	2712	wr	Mug	ref 1
T124R4	36.974	123.367	1882	gv	Haw	ref 2
T124R15	36.985	123.361	1878	wr	Mug	ref 1
T124R21	36.991	123.354	1761	wr	AB	ref 1
T124R22	36.991	123.354	1763	wr	AB	ref 1
Pioneer						
T99R1	37.342	123.445	955	wr, A	Haw	
T119R1	37.405	123.395	1494	gr	Haw	ref 1
T119R4	37.405	123.396	1439	wr	AB	ref 1
T119R5	37.405	123.397	1424	gv	Haw	ref 3
T119R9	37.403	123.399	1488	wr	Haw	ref 1
T119R10	37.402	123.400	1401	gv	AB	ref 1
T119R11	37.402	123.401	1393	gv, A	Haw	ref 1
T119R15	37.396	123.407	1040	gr, A	Mug	ref 3
T603R4	37.368	123.424	929	gv	AB	
T603R6	37.363	123.424	827	wr, A	Haw	
T604R3	37.390	123.391	1550	wr	Mug	
T604R4	37.390	123.391	1549	gr	Haw	
T604R6	37.389	123.393	1485	wr	Haw	
T604R7	37.389	123.393	1485	wr, I	Mug	
T604R8	37.389	123.393	1485	wr, A	Haw	
T604R12	37.383	123.405	1236	gv	Haw	
T627R1	37.397	123.445	1817	wr	AB	
T627R2	37.397	123.444	1761	wr, A	Haw	
T627R3	37.397	123.443	1713	wr	Haw	
T627R5	37.396	123.441	1640	wr, A	Haw	
T627R6	37.396	123.441	1625	wr	Haw	
T627R7	37.396	123.441	1619	wr, I	Haw	
T627R8	37.396	123.440	1586	wr, I	Haw	
T892R1	37.394	123.434	1315	wr	Haw	
T892R3	37.395	123.431	1243	wr/gr	Mug	
T892R5	37.395	123.430	1205	gv	Mug	
T892R7	37.394	123.428	1228	wr	AB	
T892R10	37.391	123.425	1084	gr	Mug	
T892R11	37.391	123.424	1052	gr	Mug	
T892R14	37.389	123.423	992	wr	Mug	
T892R16	37.388	123.423	979	gv	Mug	

[a] Abbreviations are as follows: wr, whole rock; gr, glass rim; gv, volcaniclastic glass; A, Ar-Ar age; I, isotope; AB, alkalic basalt; Haw, hawaiite; Mug, mugearite; Ben, benmoreite; Tra, trachyte; TB, tholeiitic basalt; Bas, basanite; calc, calc-alkaline.
[b] Ref, published analysis, numbered as follows: 1, *Davis et al.* [2002]; 2, *Davis and Clague* [2003]; 3, *Davis et al.* [2007].
[c] Glass analyses for these seven samples collected in 2009 using the ROV *Doc Ricketts* are not included in the plots or text.

Table A2 (Sample). Electron Microprobe Composition of Glasses[a] [The full Table A2 is available in the HTML version of this article]

Sample	Type	SiO_2	TiO_2	Al_2O_3	FeO*	MnO	MgO	CaO	Na_2O	K_2O	P_2O_5	S	Cl	Total
Pioneer														
T603R4a	vc	47.69	3.76	14.51	12.58	0.25	4.99	9.96	3.48	1.34	0.71	0.030	0.034	99.43
T603R4b	vc	48.33	3.58	14.69	12.11	0.24	5.22	9.95	3.43	1.20	0.62	0.023	0.029	99.49
T604R4	vc	48.11	3.44	16.80	11.32	0.24	4.15	8.97	3.98	2.35	1.00	0.029	0.061	100.53
T604R4A	vc	51.57	2.40	17.31	9.95	0.26	3.19	6.94	3.76	2.70	0.93	0.025	0.085	99.17
T604R4B	vc	51.67	2.39	17.39	10.06	0.27	3.14	6.99	4.00	2.86	0.90	0.023	0.094	99.83
T604R12	vc	48.01	3.54	16.79	11.37	0.24	4.37	9.04	4.13	2.29	0.99	0.027	0.058	100.91
T892R3	gr	49.21	3.30	16.12	10.46	0.17	3.30	7.79	4.70	2.63	0.94	0.047	0.081	98.81
T892R5	vc	49.09	3.27	16.17	10.47	0.20	3.31	7.82	4.42	2.60	0.96	0.049	0.076	98.49
T892R10a	gr	48.72	2.79	17.99	8.55	0.16	3.30	7.59	5.51	3.26	1.00	0.028	0.092	99.01
T892R10b	gr	48.72	2.76	18.00	8.58	0.14	3.30	7.60	5.54	3.26	0.94	0.033	0.086	98.99
T892R11	gr	48.33	2.75	17.94	8.62	0.15	3.31	7.60	5.45	3.25	0.92	0.031	0.099	98.47
T892R16	vc	48.35	2.75	17.71	7.94	0.15	2.96	6.64	5.65	3.66	0.96	0.029	0.094	96.89
T892R18a	vc	49.18	2.78	17.97	8.36	0.13	3.17	7.24	5.59	3.40	0.87	0.036	0.086	98.84
T892R18b	vc	49.29	2.71	18.02	8.44	0.15	3.20	7.25	5.55	3.35	0.79	0.027	0.077	98.88
T892R19	vc	49.09	2.70	18.03	8.18	0.15	3.16	7.26	5.53	3.35	0.91	0.034	0.096	98.51
T892R20	vc	47.41	3.49	16.43	10.26	0.19	3.81	8.66	4.52	2.48	0.80	0.035	0.062	98.19
T892R21	vc	46.95	3.47	16.41	10.07	0.18	3.78	8.69	4.64	2.50	0.89	0.034	0.061	97.71
T892R24	vc	47.17	3.44	16.46	10.22	0.19	3.80	8.67	4.49	2.47	0.91	0.036	0.073	97.97
T892R31	vc	48.46	3.16	17.53	9.34	0.18	3.43	7.83	5.07	3.06	0.74	0.027	0.076	98.93
T892R32	vc	49.64	3.02	15.58	9.97	0.20	2.84	6.64	4.75	2.98	0.78	0.044	0.071	96.57
T892R34	vc	47.08	3.83	15.46	11.72	0.18	4.59	9.88	3.94	1.63	0.52	0.032	0.035	98.95
T892R35	vc	47.29	3.65	16.06	11.20	0.18	4.16	9.72	3.93	1.72	0.55	0.036	0.033	98.59
T1100R1	gv	50.10	3.02	18.36	8.58	0.18	2.96	6.81	5.45	3.70	1.08	0.045	0.112	100.39
T1100R2	gr	49.98	2.97	18.34	8.59	0.17	2.96	6.89	5.42	3.62	1.09	0.053	0.110	100.18
T1100R3	gr	49.83	3.03	18.31	8.63	0.16	3.06	7.02	5.15	3.48	1.08	0.050	0.106	99.91
T1100R4	gv	49.60	3.04	17.65	9.53	0.17	3.14	7.32	4.85	3.19	1.19	0.047	0.089	99.81
T1100R6	gr	48.20	3.25	17.00	10.09	0.18	3.36	7.80	5.09	3.09	1.20	0.053	0.088	99.41
T1100R9	gr	49.20	3.60	16.08	10.87	0.20	3.45	7.94	3.68	2.82	0.97	0.058	0.072	98.94
T1101R1	gv	47.15	3.74	15.93	11.21	0.18	4.10	9.49	3.53	2.31	0.83	0.045	0.067	98.57
T1101R4	gv	46.89	3.59	15.85	11.17	0.19	4.16	9.05	3.61	2.43	0.82	0.044	0.062	97.88
T1101R5A	vc	47.32	3.72	15.96	11.16	0.18	3.86	8.95	4.04	2.56	0.93	0.045	0.068	98.80
T1101R5B	vc	47.44	3.80	15.90	11.37	0.19	3.74	8.83	4.11	2.63	0.96	0.045	0.072	99.07
T1101R7	gv	47.22	3.84	14.57	13.09	0.18	4.36	9.46	3.41	1.62	0.69	0.052	0.039	98.54
D84-R7	vc	48.61	3.80	16.09	10.48	0.20	3.47	8.01	4.31	2.89	1.25	0.047	0.079	99.25
D84-R8	vc	48.64	3.77	15.91	10.26	0.19	3.84	8.58	4.10	2.78	1.20	0.037	0.081	99.38
D84-R13	vc	46.03	3.64	16.61	10.92	0.19	3.95	9.17	4.57	2.68	1.51	0.059	0.077	99.43
D84-R14	vc	45.93	3.72	16.56	10.44	0.21	3.90	9.13	4.56	2.69	1.48	0.060	0.081	98.78
D84-R20	vc	46.98	3.96	15.59	11.68	0.20	3.80	9.04	3.71	2.38	1.01	0.054	0.070	98.49
D84-R25	vc	47.62	3.61	15.85	11.63	0.19	4.11	8.85	3.78	2.07	0.86	0.035	0.057	98.66
D84-R26	vc	47.58	3.54	15.79	11.64	0.20	4.05	8.78	3.93	2.11	0.88	0.037	0.065	98.61
Rodriguez														
T628R3A-1	vc	48.65	3.00	18.00	9.08	0.12	4.54	7.91	4.33	2.25	0.80	0.032	0.070	98.83
T628R3A-2	vc	49.39	3.32	17.14	9.82	0.15	4.24	7.97	4.05	2.41	0.90	0.028	0.090	99.51
T628R4-1	vc	49.78	2.91	17.88	9.13	0.16	4.53	7.99	4.43	2.26	0.80	0.028	0.085	99.98
T628R4-2	vc	48.97	2.54	16.94	9.80	0.14	5.28	9.51	3.94	1.82	0.60	0.032	0.060	99.67
T628R4A-1	vc	52.69	2.90	18.72	7.43	0.15	3.40	5.63	4.85	3.33	1.23	0.004	0.120	100.45
T628R4A-2	vc	48.81	2.75	17.05	9.32	0.24	5.33	9.92	3.81	1.76	0.67	0.040	0.070	99.81
T628R4A-3	vc	49.62	3.09	17.69	9.04	0.21	4.54	8.07	4.23	2.30	0.88	0.028	0.080	99.80
T628R5	vc	50.17	2.73	17.83	9.27	0.14	4.51	7.93	4.30	2.27	0.74	0.036	0.080	100.03
T628R8	vc	48.64	2.70	17.09	9.69	0.13	5.55	9.71	4.02	1.80	0.63	0.028	0.080	100.07
T628R9	vc	48.14	2.71	16.80	9.62	0.12	5.24	9.60	3.98	1.76	0.53	0.028	0.060	98.62
T628R13	vc	48.15	2.77	16.77	9.66	0.14	5.15	9.54	4.06	1.81	0.56	0.028	0.065	98.71
T628R13A	vc	47.95	2.76	16.74	9.65	0.14	5.14	9.49	4.04	1.79	0.55	0.024	0.060	98.35
T628R20	vc	49.30	2.95	17.62	9.41	0.14	4.67	8.31	4.24	2.20	0.78	0.028	0.080	99.75
T629R6A	gr	47.77	2.81	16.89	9.37	0.12	5.65	9.85	3.68	1.69	0.60	0.052	0.070	98.60
T629R6B	vc	48.07	2.79	16.99	9.50	0.15	5.65	9.75	3.68	1.76	0.65	0.048	0.070	99.17
T629R7	vc	47.88	2.80	16.91	9.49	0.15	5.66	9.78	3.7	1.69	0.64	0.052	0.060	98.86
T629R8	vc	48.16	2.63	17.33	9.38	0.14	5.75	9.78	3.63	1.64	0.59	0.052	0.050	99.20
T629R9A	vc	47.29	3.10	16.37	10.24	0.16	5.82	9.5	3.64	1.89	0.69	0.052	0.050	98.89

[a] FeO*, all iron as FeO; gr, glass rim; vc, volcaniclastic; inc, inclusion in mineral.

Table A3 (Sample). Major and Trace Element Composition of Whole Rocks[a] [The full Table A3 is available in the HTML version of this article]

	Gumdrop Seamount			Pioneer Seamount							
	T122R5	T122R9	T122R19	T99R1	T603R6	T604R3	T604R6	T604R7	T604R8	T627R1	T627R2
SiO_2 (wt %)	49.94	50.20	51.81	47.25	51.91	50.97	49.98	51.62	51.77	47.91	48.20
TiO_2	2.37	2.32	2.33	3.31	2.75	2.02	1.99	2.11	2.22	3.05	3.08
Al_2O_3	18.32	17.92	17.94	20.03	17.70	18.17	18.13	18.90	18.91	17.14	17.05
FeO*	8.34	8.43	7.92	8.80	7.88	9.63	10.62	8.09	9.36	10.82	10.29
MnO	0.10	0.10	0.32	0.14	0.13	0.17	0.16	0.12	0.10	0.15	0.15
MgO	5.61	5.66	2.82	3.03	3.66	3.64	3.62	2.46	1.84	5.62	5.48
CaO	9.26	9.04	10.58	10.09	8.71	7.53	8.27	8.61	8.72	9.47	9.31
Na_2O	3.62	3.76	3.96	4.35	4.35	4.56	4.01	4.53	3.92	3.27	3.68
K_2O	1.63	1.77	1.66	1.78	2.09	2.58	2.11	2.46	2.17	1.66	1.84
P_2O_5	0.82	0.80	0.67	1.21	0.83	0.74	1.10	1.09	0.99	0.92	0.92
XRF (ppm)											
Ni	136	139	89	21	122	41	38	24	11	86	67
Cr	209	204	209	76	89	62	61	59	66	140	121
Sc	21	21	25	19	20	16	16	17	17	21	20
V	197	192	247	237	190	150	159	162	175	216	215
Ba	489	484	244	497	453	535	576	599	575	386	376
Rb	29	33	29	27	35	57	39	52	35	21	29
Sr	586	570	455	2284	702	591	633	649	612	718	690
Zr	214	210	178	278	258	280	279	294	272	238	251
Y	28	27	30	35	34	31	30	33	31	43	30
Nb	63.7	62.2	34.8	65.6	65.3	82.9	83.1	86.8	72.7	60.1	56.5
Ga	17	17	20	19	23	20	19	21	18	20	20
Cu	46	48	32	16	30	39	34	39	25	25	32
Zn	85	78	94	93	109	94	100	85	76	114	108
IC-PMS											
La	40.24	40.03	26.67	43.90	38.20	46.36	47.27	49.58	49.28	41.72	35.73
Ce	73.26	72.26	51.44	86.60	72.49	81.87	83.74	88.02	90.31	71.19	70.57
Pr	8.37	8.33	6.36	10.58	8.88	9.37	9.52	9.99	10.44	9.23	8.76
Nd	31.84	31.51	25.90	42.06	35.48	34.36	35.03	36.93	39.17	37.60	35.53
Sm	6.37	6.35	6.03	9.21	7.99	6.79	6.94	7.31	7.77	8.56	8.05
Eu	2.11	2.04	2.02	3.06	2.58	2.08	2.11	2.24	2.44	2.70	2.69
Gd	6.05	6.08	6.18	8.72	7.53	6.05	6.06	6.40	7.26	8.24	7.96
Tb	0.92	0.91	0.96	1.31	1.11	0.89	0.90	0.95	1.09	1.20	1.19
Dy	5.49	5.37	5.62	7.48	6.22	4.99	5.09	5.33	6.31	6.73	6.71
Ho	1.08	1.06	1.10	1.42	1.15	0.95	0.97	1.03	1.25	1.28	1.25
Er	2.93	2.81	2.87	3.73	3.05	2.65	2.73	2.82	3.38	3.41	3.25
Tm	0.41	0.41	0.39	0.49	0.42	0.38	0.39	0.41	0.46	0.46	0.43
Yb	2.51	2.41	2.37	2.97	2.59	2.39	2.48	2.59	2.81	2.86	2.56
Lu	0.39	0.38	0.37	0.46	0.40	0.38	0.39	0.41	0.44	0.45	0.39
Ba	480.56	468.34	240.19	491.31	438.93	491.32	531.39	562.36	574.92	385.63	369.00
Th	5.35	5.28	2.99	4.53	3.23	4.95	5.06	5.36	6.29	2.94	3.75
Nb	67.23	66.18	37.06	71.18	62.37	78.34	74.09	80.07	76.96	62.91	60.31
Y	27.99	27.91	29.55	36.74	36.91	30.95	32.17	33.32	32.36	46.37	32.10
Hf	4.76	4.70	4.48	6.62	5.70	5.50	5.37	5.83	6.02	5.52	5.83
Ta	4.15	4.09	2.46	4.52	3.64	4.66	4.36	4.73	4.77	3.81	3.72
U	1.25	1.26	0.73	0.93	1.27	1.36	1.40	1.47	1.39	0.72	1.14
Pb	2.16	2.16	1.45	2.33	1.99	2.76	2.82	2.93	2.92	1.81	1.85
Rb	28.31	32.89	27.92	24.45	32.87	51.37	36.17	48.67	35.45	19.41	27.07
Cs	1.29	1.24	0.30	0.28	0.41	0.74	0.42	0.64	0.43	0.26	0.45
Sr	593.41	577.23	459.09	2319.53	683.78	540.47	591.37	610.95	627.26	714.45	707.33
Sc	21.31	21.32	25.50	20.10	19.40	15.49	15.81	16.56	17.61	21.57	20.70
Zr	205.69	201.93	170.31	274.51	254.96	262.11	261.46	277.77	264.86	241.71	241.63

[a] Major elements normalized to 100%. FeO*, all iron as FeO; n.r., not reported.

beneath the seamounts that does not share the metasomatic component. A process of magma generation that the postsubduction coastal volcanism and the seamounts built on abandoned spreading centers have in common is small degrees of partial melting of a variably enriched asthenospheric Pacific mantle undergoing decompression melting. The nature and amount of the enriched component may determine if and how much melt is generated. Existing zones of weakness, such as provided by the ocean crust fabric, and/or extension related to transform fault movements, may be necessary to allow eruption of small volumes of lava, especially as the degree of melting and eruption rates decrease and the melts originate deeper in the mantle.

6. Conclusions

[54] Volcanic rocks from eight structurally similar seamounts located along the continental margin offshore central to southern California are predominantly low-MgO alkalic basalt and hawaiite. More evolved mugearite, benmoreite and trachyte are less abundant. Tholeiitic basalt and basanite were each recovered from only one seamount. Except for the crystallized benmoreite and trachyte, the same compositional range observed for whole-rock samples is present as glass, either as pillow rims or as volaniclastic breccia, pumice clasts, or sand grains. Sulfur contents of the most glasses indicate significant degassing, compatible with eruption in shallow water or above sea level when several of the seamounts were islands. Trace element abundances and ratios are typical for ocean island basalts and all are LREE enriched, even the tholeiitic samples, although to a lesser degree. Isotopic compositions range from MORB-like to relatively enriched OIB, similar to lavas from other seamounts and islands in the eastern Pacific Ocean. Isotopic compositions and incompatible elements are not well correlated and suggest an origin by variable degrees of partial melting of a variably enriched mantle source.

[55] High-precision $^{40}Ar/^{39}Ar$ ages indicate multiple episodes of volcanism occurred with the most voluminous eruptions between 16 to 7 Ma. A young age of 2.8 Ma for the basanite from San Juan suggests volcanism persisted into more recent times. A comparable suite of lava compositions erupted over the same long time span on Davidson [*Clague et al.*, 2009b], atop a known fossil spreading center, which suggests a common origin for these continental margin volcanoes. Ultimately, the continental margin volcanoes, as well as chemically similar Miocene volcanic units onshore, owe their origin to the changes from a subduction to a transform plate margin. Decompression melting of enriched parts of the underlying sub-Pacific mantle produced small volumes of melt that rose along zones of weakness, probably aided by transtensional faulting along the continental margin.

Appendix A

[56] Table A1 summarizes the location, depth, analyses, rock type, and lists references for analyses that were published previously. Table A2 gives the electron microprobe composition of glasses, and Table A3 provides the major and trace element composition of whole rocks.

Acknowledgment

[57] We thank the ROV *Tiburon* pilots and captain and crew of the R/V *Western Flyer* for their skillful recovery of the samples. We thank Charlie Paull and Tessa Hill for additional samples collected on their dives to Pioneer Seamount. The 1969 R/V *Agassiz* samples were archived at Scripps Institution of Oceanography for the intervening 40 years. Robert Oscarson assisted with microprobe analysis. The support of the David and Lucile Packard Foundation through a grant to MBARI is gratefully acknowledged. Constructive criticism by Jim Natland and an especially thorough and helpful anonymous review improved the manuscript.

References

Atwater, T. (1970), Implications of plate tectonics for the Cenozoic tectonic evolution of western North America, *Geol. Soc. Am. Bull.*, *81*, 3513–3536, doi:10.1130/0016-7606(1970)81[3513:IOPTFT]2.0.CO;2.

Atwater, T. (1989), Plate tectonics history of the northeast Pacific and western North America, in *The Geology of North America*, vol. N, *The Eastern Pacific Ocean and Hawaii*, edited by E. L. Winterer, D. M. Hussong, and R. W. Decker, pp. 21–72, Geol. Soc. of Am., Boulder, Colo.

Atwater, T., and J. Severinghaus (1989), Tectonic maps of the northeast Pacific, in *The Geology of North America*, vol. N, *The Eastern Pacific Ocean and Hawaii*, edited by E. L. Winterer, D. M. Hussong, and R. W. Decker, pp. 15–20, Geol. Soc. of Am., Boulder, Colo.

Batiza, R. (1977a), Oceanic crustal evolution: Evidence from the petrology and geochemistry of isolated oceanic central volcanoes, Ph.D. thesis, 295 pp., Univ. of Calif., San Diego, La Jolla.

Batiza, R. (1977b), Petrology and geochemistry of Guadalupe Island: An alkalic seamount on a fossil ridge crest, *Geology*, *5*, 760–764, doi:10.1130/0091-7613(1977)5<760:PACOGI>2.0.CO;2.

Batiza, R., and D. Vanko (1984), Petrology of young Pacific seamounts, *J. Geophys. Res.*, *89*, 11,235–11,260, doi:10.1029/JB089iB13p11235.

Batiza, R., and D. Vanko (1985), Petrologic evolution of large failed rifts in the eastern Pacific: Petrology of volcanic rocks from the Mathematician Ridge area and the Guadalupe Trough, *J. Petrol.*, *26*, 564–602.

Batiza, R., T. J. Bernatowicz, C. M. Hohenberg, and F. A. Podosek (1979), Relations of noble gas abundances to petrogenesis and magmatic evolution of some oceanic basalts and related differentiated volcanic rocks, *Contrib. Mineral. Petrol.*, *69*, 301–313, doi:10.1007/BF00372332.

Bender, J. F., F. N. Hodges, and A. E. Bence (1978), Petrogenesis of basalts from the project FAMOUS area: Experimental studies from 0 to 15 kilobars, *Earth Planet. Sci. Lett.*, *41*, 277–302, doi:10.1016/0012-821X(78)90184-X.

Benoit, M., A. Aguillon-Robles, T. Calmus, R. C. Maury, H. Bellon, J. Cotten, J. Bourgois, and F. Michaud (2002), Geochemical diversity of late Miocene volcanism in southern Baja California, Mexico: Implication of mantle and crustal sources during the opening of an asthenospheric window, *J. Geol.*, *110*, 627–648, doi:10.1086/342735.

Bohrson, W. A., and A. S. Davis (1994), $^{40}Ar/^{39}Ar$ laser fusion ages of feldspars from volcanic rocks from seamounts offshore southern and peninsular California, *U.S. Geol. Surv. Open File Rep.*, *94-587*, 20 pp.

Bohrson, W. A., and M. R. Reid (1995), Petrogenesis of alkaline basalts from Socorro Island, Mexico: Trace element evidence for contamination of ocean island basalt in the shallow ocean crust, *J. Geophys. Res.*, *100*, 24,555–24,576, doi:10.1029/95JB01483.

Bohrson, W. A., and M. R. Reid (1997), Genesis of silicic peralkaline volcanic rocks in an ocean island setting by crustal melting and open-system processes: Socorro Island, Mexico, *J. Petrol.*, *38*, 1137–1166, doi:10.1093/petrology/38.9.1137.

Bohrson, W. A., M. R. Reid, A. Grunder, M. T. Heizler, T. M. Harrison, and J. Lee (1996), Prolonged history of silicic peralkaline volcanism in the eastern Pacific Ocean, *J. Geophys. Res.*, *101*, 11,457–11,474, doi:10.1029/96JB00329.

Castillo, P.R., E. Klein, J. Bender, C. Langmuir, S. Shirey, R. Batiza, and W. White (2000), Petrology and Sr, Nd, and Pb isotope geochemistry of mid-ocean ridge basalt glasses from the 11°45′N to 15°00′N segment of the East Pacific Rise,, *Geochem. Geophys. Geosyst.*, *1*(11), 1011, doi:10.1029/1999GC000024.

Castillo, P. R., D. A. Clague, A. S. Davis, and P. F. Lonsdale (2010), Petrogenesis of Davidson Seamount lavas and its implications for fossil spreading center and intraplate magmatism in the eastern Pacific, *Geochem. Geophys. Geosyst.*, *11*, Q02005, doi:10.1029/2009GC002992.

Church, S. E., and M. Tatsumoto (1975), Lead isotope relations in oceanic ridge basalts from the Juan de Fuca-Gorda Ridge area, N.E. Pacific Ocean, *Contrib. Mineral. Petrol.*, *53*, 253–279, doi:10.1007/BF00382443.

Clague, D. A., and G. B. Dalrymple (1987), The Hawaiian-Emperor volcanic chain, part I: Geological evolution, in *Volcanism in Hawaii*, edited by R. Decker et al., *U.S. Geol. Surv. Prof. Pap.*, *1350(1)*, 5–54.

Clague, D. A., J. R. Reynolds, and A. S. Davis (2000), Near-ridge seamounts chains in the northeastern Pacific Ocean, *J. Geophys. Res.*, *105*, 16,541–16,561, doi:10.1029/2000JB900082.

Clague, D. A., A. S. Davis, and J. E. Dixon (2003), Submarine strombolian eruptions on the Gorda mid-ocean ridge, in *Explosive Subaqueous Volcanism*, *Geophys. Monogr. Ser.*, vol. 140, edited by J. D. L. White, J. L. Smellie, and D. A. Clague, pp. 111–128, AGU, Washington, D. C.

Clague, D. A., J. B. Paduan, and A. S. Davis (2009a), Widespread strombolian eruptions of mid-ocean ridge basalt, *J. Volcanol. Geotherm. Res.*, *180*, 171–188, doi:10.1016/j.jvolgeores.2008.08.007.

Clague, D. A., J. B. Paduan, R. A. Duncan, J. J. Huard, A. S. Davis, P. R. Castillo, P. Lonsdale, and A. DeVogelaere (2009b), Five million years of compositionally diverse, episodic volcanism: Construction of Davidson Seamount atop an abandoned spreading center, *Geochem. Geophys. Geosyst.*, *10*, Q12009, doi:10.1029/2009GC002665.

Cole, R. B., and A. R. Basu (1992), Middle Tertiary volcanism during ridge-trench interactions in western California, *Science*, *258*, 793–796, doi:10.1126/science.258.5083.793.

Cole, R. B., and A. R. Basu (1995), Nd-Sr isotopic geochemistry and tectonics of ridge subduction and middle Cenozoic volcanism in western California, *Geol. Soc. Am. Bull.*, *107*, 167–179, doi:10.1130/0016-7606(1995)107<0167:NSIGAT>2.3.CO;2.

Cousens, B. L. (1996), Magmatic evolution of Quaternary mafic magmas at Long Valley caldera and Devils Postpile, California: Effects of crustal contamination on lithospheric mantle-derived magmas, *J. Geophys. Res.*, *101*, 27,673–27,689, doi:10.1029/96JB02093.

Cox, K. G., J. D. Bell, and R. J. Pankhurst (1979), *The Interpretation of Igneous Rocks*, 450 pp., Allen and Unwin, London.

Davis, A. S., and D. A. Clague (1987), Geochemistry, mineralogy, and petrogenesis of basalt from the Gorda Ridge, *J. Geophys. Res.*, *92*, 10,467–10,483, doi:10.1029/JB092iB10p10467.

Davis, A. S., and D. A. Clague (1990), Gabbroic xenoliths from the northern Gorda Ridge: Implications for magma chamber processes under slow spreading ridges, *J. Geophys. Res.*, *95*, 10,885–10,905.

Davis, A. S., and D. A. Clague (2000), President Jackson Seamounts, northern Gorda Ridge: Tectonomagmatic relationship between on- and off-axis volcanism, *J. Geophys. Res.*, *105*, 27,939–27,956, doi:10.1029/2000JB900291.

Davis, A. S., and D. A. Clague (2003), Hyaloclastite from Miocene seamounts offshore central California: Compositions, eruption styles, and depositional processes, in *Explosive Subaqueous Volcanism*, *Geophys. Monogr. Ser.*, vol. 140, edited by J. D. L. White, J. L. Smellie, and D. A. Clague, pp. 129–142, AGU, Washington, D. C.

Davis, A. S., D. A. Clague, and W. F. Friesen (1994), Petrology and mineral chemistry of basalt from Escanaba Trough, southern Gorda Ridge, *U.S. Geol. Surv. Bull.*, *2022*, 153–170.

Davis, A. S., S. H. Gunn, W. A. Bohrson, L. B. Gray, and J. R. Hein (1995), Chemically diverse sporadic volcanism at seamounts offshore southern and Baja California, *Geol. Soc. Am. Bull.*, *107*, 554–570, doi:10.1130/0016-7606(1995)107<0554:CDSVAS>2.3.CO;2.

Davis, A. S., D. F. Siems, and W. A. Bohrson (1996), Volcanic rocks from Rocas Alijos, in *Rocas Alijos, Scientific Results of the Cordell Expedition*, edited by R. W. Schmieder, *Monogr. Biol.*, vol. 75, pp. 75–91, Kluwer Acad., Dordrecht, Netherlands.

Davis, A. S., D. A. Clague, and W. M. White (1998), Geochemistry of basalt from Escanaba Trough: Evidence for sediment contamination, *J. Petrol.*, *39*, 841–858, doi:10.1093/petrology/39.5.841.

Davis, A. S., D. A. Clague, W. A. Bohrson, G. B. Dalrymple, and H. G. Greene (2002), Seamounts at the continental margin of California: A different kind of oceanic volcanism, *Geol. Soc. Am. Bull.*, *114*, 316–333, doi:10.1130/0016-7606(2002)114<0316:SATCMO>2.0.CO;2.

Davis, A. S., D. A. Clague, and J. B. Paduan (2007), Diverse origins of xenoliths from seamounts at the continental

margin, offshore central California, *J. Petrol.*, *48*, 829–852, doi:10.1093/petrology/egm003.

Davis, A. S., D. A. Clague, B. L. Cousens, R. Keaten, and J. B. Paduan (2008), Geochemistry of basalt from the North Gorda segment of the Gorda Ridge: Evolution toward ultra-slow spreading ridge lavas due to decreasing magma supply, *Geochem. Geophys. Geosyst.*, *9*, Q04004, doi:10.1029/2007GC001775.

Dickinson, W. R. (1997), Overview: Tectonic implications of Cenozoic volcanism in coastal California, *Geol. Soc. Am. Bull.*, *109*, 936–954, doi:10.1130/0016-7606(1997)109<0936:OTIOCV>2.3.CO;2.

Duncan, R. A., and R. A. Keller (2004), Radiometric ages for basement rocks from the Emperor Seamounts, ODP Leg 197, *Geochem. Geophys. Geosyst.*, *5*, Q08L03, doi:10.1029/2004GC000704.

Gee, J., H. Staudigel, and J. H. Natland (1991), Geology and petrology of Jasper Seamount, *J. Geophys. Res.*, *96*, 4083–4105, doi:10.1029/90JB02364.

Ghiorso, M. S., and R. O. Sack (1995), Chemical mass transfer in magmatic processes IV: A revised and internally consistent thermodynamic model for the interpolation and extrapolation of liquid-solid equilibria in magmatic systems at elevated temperatures and pressures, *Contrib. Mineral. Petrol.*, *119*, 197–212, doi:10.1007/BF00307281.

Graham, D. W., A. Zindler, M. D. Kurz, W. J. Jenkins, R. Batiza, and H. Staudigel (1988), He, Pb, Sr and Nd isotope constraints on magma genesis and mantle heterogeneity beneath young Pacific seamounts, *Contrib. Mineral. Petrol.*, *99*, 446–463, doi:10.1007/BF00371936.

Haase, K. M., C. W. Devey, D. F. Mertz, P. Stoffers, and D. Garbe-Schoenberg (1996), Geochemistry of lavas from Mohns Ridge, Norwegian-Greenland Sea: Implications for melting conditions and magma sources near Jan Mayen, *Contrib. Mineral. Petrol.*, *123*, 223–237, doi:10.1007/s004100050152.

Haase, K. M., C. W. Devey, and M. Wienke (2003), Magmatic processes and mantle heterogeneity beneath the slow-spreading Kolbeinsey Ridge segment, North Atlantic, *Contrib. Mineral. Petrol.*, *144*, 428–448.

Hawkins, J. W., E. C. Allison, and D. MacDougall (1971), Volcanic petrology and geologic history of Northeast Bank, southern California borderland, *Geol. Soc. Am. Bull.*, *82*(1), 219–227, doi:10.1130/0016-7606(1971)82[219:VPAGHO]2.0.CO;2.

Hellebrand, E., J. E. Snow, H. J. B. Dick, and A. Hofmann (2001), Coupled major and trace elements as indicators of extent of melting in mid-ocean ridge peridotites, *Nature*, *410*, 677–681, doi:10.1038/35070546.

Johnson, D. M., P. R. Hooper, and R. M. Conrey (1999), XRF analysis of rocks and minerals for major and trace elements on a single low dilution Li-tetraborate fused bead, *Adv. X Ray Anal.*, *41*, 843–867.

Knaack, C., S. Cornelius, and P. R. Hooper (1994), Trace element analysis of rocks and minerals by ICP-MS, open file report, Dep. of Geol., Wash. State Univ., Pullman.

Konter, J. G., H. Staudigel, J. Blichert-Toft, B. B. Hanan, M. Polve, G. R. Davies, N. Shimizu, and P. Schiffman (2009), Geochemical stages at Jasper Seamount and the origin of intraplate volcanoes, *Geochem. Geophys. Geosyst.*, *10*, Q02001, doi:10.1029/2008GC002236.

Koppers, A. A. P. (2002), ArArCALC—Software for $^{40}Ar/^{39}Ar$ age calculations, *Comput. Geosci.*, *28*, 605–619, doi:10.1016/S0098-3004(01)00095-4.

Koppers, A. A. P., H. Staudigel, and J. R. Wijbrans (2000), Dating crystalline groundmass separates of altered Cretaceous seamount basalts by the $^{40}Ar/^{39}Ar$ incremental heating technique, *Chem. Geol.*, *166*, 139–158, doi:10.1016/S0009-2541(99)00188-6.

Koppers, A. A. P., H. Staudigel, and R. A. Duncan (2003), High-resolution $^{40}Ar/^{39}Ar$ dating of the oldest oceanic basement basalts in the western Pacific basin, *Geochem. Geophys. Geosyst.*, *4*(11), 8914, doi:10.1029/2003GC000574.

Lonsdale, P. (1991), Structural patterns of the Pacific floor offshore of peninsular California, in *The Gulf and Peninsular Province of the Californias*, edited by J. P. Dauphin, G. Ness, and B. R. T. Simoneit, *AAPG Mem.*, *47*, 87–125.

Mahood, G. A., and D. R. Baker (1986), Experimental constraints on depths of fractionation of mildly alkalic basalts and associated felsic rocks: Pantelleria, Strait of Sicily, *Contrib. Mineral. Petrol.*, *93*, 251–264, doi:10.1007/BF00371327.

MBARI Mapping Team (2001), MBARI west coast seamounts and ridges multibeam survey, *Digital Data Ser., 7*, Monterey Bay Aquarium Res. Inst., Moss Landing, Calif.

Mühe, R., H. Bohrman, and D. Garbe-Schoenberg (1997), E-MORB glasses from the Gakkel Ridge (Arctic Ocean) at 87°N: Evidence for the Earth's most northerly volcanic activity, *Earth Planet. Sci. Lett.*, *152*, 1–9, doi:10.1016/S0012-821X(97)00152-0.

Naumann, T. R., and D. J. Geist (1999), Generation of alkalic basalt by crystal fractionation of tholeiitic magma, *Geology*, *27*, 423–426, doi:10.1130/0091-7613(1999)027<0423:GOABBC>2.3.CO;2.

Nekvasil, H., A. Dondolini, J. Horn, J. Filiberto, H. Long, and D. H. Lindsley (2004), The origin and evolution of silica-saturated alkalic suites: An experimental study, *J. Petrol.*, *45*, 693–721, doi:10.1093/petrology/egg103.

Nicholson, C., C. C. Sorlien, T. Atwater, J. C. Crowell, and B. P. Luyendyk (1994), Microplate capture, rotation of the western Transverse Ranges, and initiation of the San Andreas transform as a low-angle fault system, *Geology*, *22*, 491–495, doi:10.1130/0091-7613(1994)022<0491:MCROTW>2.3.CO;2.

Niu, Y., K. D. Collerson, R. Batiza, J. I. Wendt, and M. Regelous (1999), Origin of enriched-type mid-ocean ridge basalt at ridges far from mantle plumes: The East Pacific Rise at 11°20′N, *J. Geophys. Res.*, *104*, 7067–7087, doi:10.1029/1998JB900037.

Paduan, J. B., D. A. Clague, and A. S. Davis (2007), Erratic continental rocks on volcanic seamounts off the US west coast, *Mar. Geol.*, *246*, 1–8, doi:10.1016/j.margeo.2007.07.007.

Paduan, J. B., D. A. Clague, and A. S. Davis (2009), Evidence that three seamounts off Southern California were ancient islands, *Mar. Geol.*, *265*, 146–156, doi:10.1016/j.margeo.2009.07.003.

Palmer, H. D. (1964), Marine geology of Rodriguez Seamount, *Deep Sea Res.*, *11*, 737–756.

Perfit, M. R., D. J. Fornari, A. Malahoff, and R. W. Embley (1983), Geochemical studies of abyssal lavas recovered by DSRV *Alvin* from eastern Galapagos rift, Inca transform and Ecuador rift: 3. Trace element abundances and petrogenesis, *J. Geophys. Res.*, *88*, 10,551–10,572, doi:10.1029/JB088iB12p10551.

Pringle, M. S., H. Staudigel, and J. Gee (1991), Geochronology of Jasper Seamount: Seven million years of volcanism, *Geology*, *19*, 364–368, doi:10.1130/0091-7613(1991)019<0364:JSSMYO>2.3.CO;2.

Renne, P. R., C. C. Swisher, A. L. Deino, D. B. Karner, T. L. Owens, and D. J. DePaolo (1998), Intercalibration of standards, absolute ages and uncertainties in $^{40}Ar/^{39}Ar$ dating, *Chem. Geol.*, *145*, 117–152, doi:10.1016/S0009-2541(97)00159-9.

Siebe, C. J., C. Komorowski, C. Navarro, J. McHone, H. Delgado, and A. Cortes (1995), Submarine eruption near Socorro Island, Mexico: Geochemistry and scanning electron microscopy studies of floating scoria and reticulite, *J. Volcanol. Geotherm. Res.*, *68*, 239–271, doi:10.1016/0377-0273(95)00029-1.

Smith, J. R., and R. Batiza (1989), New field and laboratory evidence for the origin of hyaloclastite flows on seamount summits, *Bull. Volcanol.*, *51*, 96–114, doi:10.1007/BF01081979.

Sun, S. S., and W. F. McDonough (1989), Chemical and isotopic systematics of oceanic basalts: Implications for mantle composition and processes, in *Magmatism in the Ocean Basins*, edited by A. D. Saunders and M. J. Norry, *Geol. Soc. Spec. Publ.*, *42*, 313–345.

Todt, W., R. A. Cliff, A. Hanser, and A. W. Hofmann (1984), ^{202}Pb-^{205}Pb spike for Pb isotopic analysis, *Terra Cognita*, *4*, 209.

Weigand, P. W., K. L. Savage, and C. C. Nicholson (2002), The Conejo Volcanics and other Miocene volcanic suites in southwestern California, in *Crustal Evolution of the Southwestern United States*, edited by A. Barth, *Geol. Soc. Am. Spec. Pap., 365*, 187–204.

White, W. M., A. W. Hofmann, and H. Puchelt (1987), Isotope geochemistry of Pacific mid-ocean ridge basalt, *J. Geophys. Res.*, *92*, 4881–4893, doi:10.1029/JB092iB06p04881.

Zindler, A., H. Staudigel, and R. Batiza (1984), Isotope and trace element geochemistry of young Pacific seamounts: Implications for the scale of upper mantle heterogeneity, *Earth Planet. Sci. Lett.*, *70*, 175–195, doi:10.1016/0012-821X(84)90004-9.